AGU PUBLICATIONS

Geochemistry, Geophysics, Geosystems

RESEARCH ARTICLE
10.1002/2015GC005937

Variations of the lithospheric strength and elastic thickness in North America

Magdala Tesauro[1,2], Mikhail K. Kaban[2], and Walter D. Mooney[3]

[1]Department of Earth Sciences, Utrecht University, Utrecht, Netherlands, [2]Helmholtz-Zentrum Potsdam, Deutsches GeoForschungsZentrum GFZ, Germany, [3]U.S. Geological Survey, Menlo Park, California, USA

Key Points:
- We estimate strength and T_e distribution of the North American continent
- Thermal more than compositional changes induce main strength and T_e variations
- Seismicity is concentrated where large contrast of strength is estimated

Supporting Information:
- Supporting Information S1

Correspondence to:
M. Tesauro,
M.Tesauro@uu.nl

Citation:
Tesauro, M., M. K. Kaban, and W. D. Mooney (2015), Variations of the lithospheric strength and elastic thickness in North America, *Geochem. Geophys. Geosyst.*, *16*, 2197–2220, doi:10.1002/2015GC005937.

Received 1 JUN 2015
Accepted 7 JUN 2015
Accepted article online 11 JUN 2015
Published online 14 JUL 2015

Abstract We evaluate the effect of temperature variations on strength and effective elastic thickness (T_e) of the lithosphere of the North American (NA) continent. To this purpose, we use two thermal models that are corrected for compositional variations and anelasticity effects in the upper mantle. These thermal models are obtained from a joint inversion of gravity data and two recent seismic tomography models (NA07 and SL2013sv). The crustal rheology was defined using NACr14, the most recent NA crustal model. This model specifies seismic velocities and thickness for a three-layer model of the crystalline crust. Strength in the lithosphere and in the crust has similar distributions, indicating that local geotherms play a dominant role in determining strength rather than crustal composition. A pronounced contrast is present in strength between cratonic and off-cratonic regions. Lithospheric strength in the off-cratonic regions is prevalently localized within the crust and T_e shows low values (<20 km), while the inner part of the cratons is characterized by a strong lithosphere with large T_e (>150 km). In contrast to previous results, our models indicate that Phanerozoic regions located close to the edge of the cratons, as the Appalachians, are characterized by low strength. We also find that locally weak zones exist within the cratons (e.g., beneath the intracratonic Illinois Basin and Midcontinent rift). Seismic tomography models NA07 and SL2013sv differ mainly in some peripheral parts of the cratons, as the Proterozoic Canadian Platform, the Grenville, and the western part of the Yavapai-Mazatzal province, where the integrated strength for the model NA07 is 10 times larger than in model SL2013sv due to a temperature difference (>200°C) in the uppermost mantle. The differences in T_e between the two models are less pronounced. In both models, Proterozoic regions reactivated by Meso-Cenozoic tectonics (e.g., Rocky Mountains and the Mississippi Embayment) are characterized by a weak lithosphere due to the absence of the mechanically strong part of the mantle lithospheric layer. Intraplate earthquakes are distributed along the edges of the cratons, demonstrating that tectonic stress accumulates there, while the cores of the cratons remain undeformed. In both models, intraplate earthquakes occur in weak lithosphere ($\sim 0.5 \times 10^{13}$ Pa s, $T_e \sim 15$ km) or near the edges of strong cratonic blocks, characterized by pronounced contrasts of strength and T_e.

1. Introduction

The long-term rheological properties of the lithosphere are fundamental for understanding both crustal tectonics and mantle dynamics. For a given mineralogical composition and microstructure, the most important parameters that control rock rheology are pressure, temperature, strain (including strain rate and history), fluid content and pore fluid pressure, grain size, fugacities of volatiles, and the chemical activities of mineral components [e.g., *Evans and Kohlstedt*, 1995]. At larger scale, the strength of the lithosphere mainly depends on its temperature, composition, tectonic setting, and factors that define the other critical parameters, such as strain rate and availability of fluids. The effective elastic thickness of the lithosphere (T_e), characterizing its response to loading [e.g., *Watts and Burov*, 2003], is an important parameter that is related to strength. T_e reflects the long-term and often complex history of the continental plate and depends primarily on the combined effects of rheological and thermal heterogeneity. The latter in particular controls the coupling or decoupling conditions of the lithospheric layers [e.g., *Burov and Diament*, 1995; *Burov*, 2011; *Cloetingh and Burov*, 2011], and thus relates T_e to the style of lithospheric deformation in response to stresses.

T_e has traditionally been inferred from the response of the lithosphere to tectonic stresses and vertical loads, e.g., through cross-spectral analyses of the gravity field and topography [e.g., *Bechtel et al.*, 1990; *Pilkington*, 1991; *Wang and Mareschal*, 1999; *Armstrong and Watts*, 2001; *Flück et al.*, 2003; *Kirby and Swain*, 2009; *Audet*

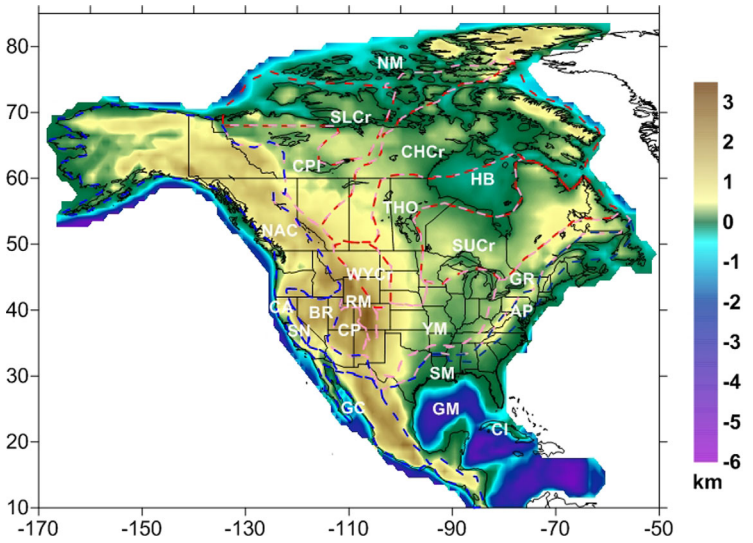

Figure 1. Topographic map of North America (km). Red, pink, and blue-dashed contours show the boundaries between the Archean, Proterozoic, and Phanerozoic tectonic provinces. White labels stand as follows: AP, Appalachians; BR, Basin and Range; CA, Cascade; CHCr, Churchill craton; CI, Cuba Island; CP, Colorado Plateau; CPl, Canadian Platform; GC, Gulf of California; GM, Gulf of Mexico; GR, Grenville; HB, Hudson Basin; NAC, North American Cordillera; NM, North Margin; RM, Rocky Mountains; SLCr, Slave craton; SM, South Margin; SN, Sierra Nevada; SUCr, Superior craton; THO, Trans-Hudson Orogen; WYCr, Wyoming Craton; YM, Yavapai-Mazatzal province.

and Mareschal, 2004a,b, 2007; *Poudjom Djomani et al*., 2005; *Audet and Bürgmann*, 2011; *Kirby and Swain*, 2014]. This method employs measures of the relationship between the observed gravity and topography in the spectral domain, namely the admittance and coherence. Various approaches are used to calculate these parameters [see *Kirby*, 2014, for a review], such as the maximum entropy method [e.g., *Lowry and Smith*, 1995; *Wang and Mareschal*, 1999; *Armstrong and Watts*, 2001; *Flück et al*., 2003; *Audet and Mareschal*, 2004a], periodograms [e.g., *Bechtel et al*., 1990; *Pilkington*, 1991; *Poudjom Djomani et al*., 2005], multitaper [*Audet and Mareschal*, 2004b], and wavelets transform [e.g., *Audet et al*., 2007; *Audet and Mareschal*, 2007; *Audet and Bürgmann*, 2011]. However, the results of these studies may be sometimes biased by several factors and simplifying assumptions, such as that the lithosphere consists of a homogeneous and continuous plate. This can lead to inconsistent estimates of T_e [*Artemjev and Kaban*, 1991; *Kirby*, 2014]. In particular, T_e estimates for cratons based on the transfer function (admittance) of the free air gravity and topography are in some cases significantly lower than the values obtained from the coherence analysis of the Bouguer anomalies and topography [*McKenzie*, 2003]. Indeed, the latter method employs decomposition of the load into surface and internal components and is less sensitive to short-wavelength noise in the data than the admittance technique.

In previous studies, the strength and T_e of the lithosphere were estimated on a global [*Tesauro et al*., 2012a, 2013] and regional scale [*Cloetingh et al*., 2005; *Tesauro et al*., 2009a, 2009b; *Hardebol et al*., 2013] on the basis of lithospheric thermorheological models. The robustness of these results is mainly determined by the accuracy of the compositional and thermal models used as input. To this purpose, *Tesauro et al*. [2013] investigated the influence of the crustal composition on the strength and T_e by constructing a set of possible end-member strength models, using "soft" and "hard" rheology for the continental crust. They found that the largest differences between the end-member models in terms of the estimated strength and T_e distributions are for the areas characterized by an "intermediate" thermal regime. Therefore, in these regions uncertainties in factors other than temperature estimates play a significant role in determining strength.

In this study, we evaluate the effect of temperature variations on lithospheric strength and T_e of the North American (NA) continent (see Appendix A for description of the method). The study area comprises tectonic provinces of different age (Figure 1) that have been the target of a large number of deep crustal and lithospheric observational studies (e.g., Lithoprobe, http://earthsciencescanada.com). To reach our goal, we use the two new thermal models presented by *Tesauro et al*. [2014a] which were obtained through a joint inversion of gravity and seismic tomography data [*Kaban et al*., 2014]. Our results are also relevant in view of longstanding debates on the strength distribution in the continental lithosphere, in particular whether or

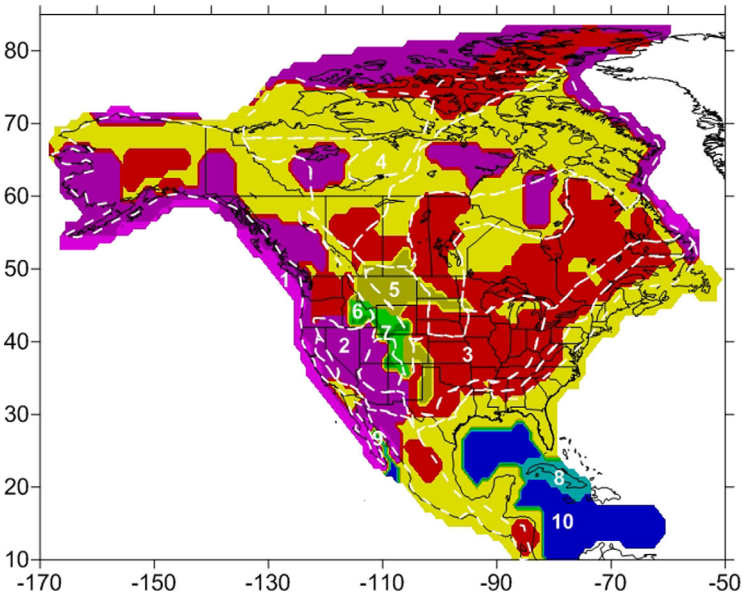

Figure 2. Rheological types of crustal layers, assigned on the basis of the crustal seismic velocity variations estimated in NACr14 [*Tesauro et al*., 2014b], are identified by colors and white numbers defined in Table 1. White-dashed contours show the boundaries between the tectonic provinces as in Figure 1. See text for further explanation.

not the strength resides primarily in the crust and thus the role that lithospheric mantle plays in controlling T_e [e.g., *McKenzie and Fairhead*, 1997; *Jackson*, 2002; *Afonso and Ranalli*, 2004; *Burov*, 2010]. In addition, we examine the difference between the two models of strength and T_e in comparison with spatial distribution of intraplate earthquakes. We evaluate the hypothesis, derived from a joint analysis of global seismicity and lithospheric shear velocities, that a large number of intraplate earthquakes occur in areas characterized by lower lithospheric strength and/or higher stress concentration compared to typical intraplate settings [*Mooney et al*., 2012].

2. Rheological and Thermal Models of the NA Lithosphere

The determination of the 3-D thermal and compositional structure of the NA continental lithosphere has been a primary aim of extensive geophysical surveys [e.g., *Currie and Hyndman*, 2006; *Clowes et al*., 1995, 2010]. In this study, we define the crustal rheology using as input the model NACr14, the most recent crustal seismic velocity model of the NA continent [*Tesauro et al*., 2014b]. NACr14 provides *P* wave seismic velocities and the thickness of the crystalline crustal layers based on the most comprehensive compilation of seismic data [USGS database, *Mooney*, 2015].

Laboratory measurements, which have more control on the uncertainties of the rheological parameters [e.g., *Bürgmann and Dresen*, 2008], utilize simple monophase minerals with a homogeneous grain size, whose applicability to real aggregate compositions remains to be demonstrated. For this reason, in assigning the crustal rheology, we prefer to use the results of the experiments carried out on natural samples [e.g., *Carter and Tsenn*, 1987; *Wilks and Carter*, 1990]. In particular, we use the results of the experiments performed on rocks in "wet" and "dry" conditions representing weak ("soft") and strong ("hard") crustal rheology. By making this choice, we do not intend to refer to the (an)hydrate conditions of the crust, neither to represent the diversity of the crustal rock types, but rather to relate crustal physical parameters (velocity in this case) to a specific rheology.

According to NACr14, we assign the "hard" rheology, corresponding to crustal layers consisting of granite-diabase-mafic granulite, to regions characterized by high crustal seismic velocities (e.g., the northern Rocky Mountains) and the "soft" rheology, corresponding to crustal layers consisting of quartzite-diorite, to regions with low crustal seismic velocities (e.g., some continental margins). Between these two end-members, we define several other rheologies given by a combination of these lithologies, as assigned to the areas with intermediate crustal seismic velocities (Figure 2 and Table 1). In this way, we define seven crustal rheologies

Table 1. Rheology and Young's Modulus (E) Assigned to the Upper (UC), Middle (MC), and Lower Crust (LC), According to the Corresponding Range of Velocities Estimated in NACr14 [*Tesauro et al*., 2014b][a]

Code	Velocity (km/s) UC	Velocity (km/s) MC	Velocity (km/s) LC	Rheology/E (GPa) UC	Rheology/E (GPa) MC	Rheology/E (GPa) LC
1	5.80–6.0	6.20–6.60	6.40–6.60	Dry Quartzite/93	Wet Diorite/99	Wet Diorite/99
2	5.80–6.0	6.20–6.60	6.60–6.90	Dry Quartzite/93	Wet Diorite/99	Dry Diabase/106
3	6.0–6.30	6.20–6.60	6.90–7.40	Dry Granite/88	Wet Diorite/99	Mafic Granulite/110
4	6.0–6.30	6.20–6.60	6.60–6.90	Dry Granite/88	Wet Diorite/99	Dry Diabase/106
5	6.0–6.30	6.60–6.85	6.90–7.40	Dry Granite/88	Dry Diabase/106	Mafic Granulite/110
6	5.80–6.0	6.60–6.85	6.90–7.40	Dry Quartzite/88	Dry Diabase/106	Dry Diabase/106
7	5.80–6.0	6.20–6.60	6.90–7.40	Dry Quartzite/93	Wet Diorite/99	Mafic Granulite/110
8	6.0–6.30		6.90–7.40	Dry Granite/88		Mafic Granulite/110
9	5.50–5.80		6.40–6.60	Wet Quartzite/93		Wet Diorite/99
10	6.5–6.70			Diabase/106		

[a]Rheological types from 1 to 7 are assigned to regions in which the crust is divided in three layers, while from 8 to 9 those in which the crust is divided in two layers and 10 those with only one crustal layer. Rheological model parameters are displayed in Table A1.

in regions where the crust is divided in three layers, and two crustal rheologies in regions where the crystalline crust consists of two layers. The rheology of diabase is assigned to the Gulf of Mexico with one crystalline crust layer of an oceanic type (Table 1). We do not specify any rheology for sediments, because they are normally affected only by brittle deformation, while in the mantle lithosphere we assume a uniform "dry" olivine/peridotite rheology. A "wet" mantle model might be suitable for areas recently affected by subduction of oceanic lithosphere and tectonothermal events and would further lower the lithospheric strength [e.g., *Afonso and Ranalli*, 2004]. Unfortunately, the low temperature-plasticity law has been determined only for "dry" conditions [*Mei et al*., 2010]. This assumption likely does not affect the results significantly, since the areas of the NA continent characterized by a "wet" mantle are of a Phanerozoic age or correspond to the west coast and perhaps parts of the craton which have been rejuvenated by refertilization events. In these regions, the temperatures of the shallowest part of the upper mantle (<100 km) are close to the melting point [*Tesauro et al*., 2014a], and thus the strength will be prevalently concentrated in the crust. Indeed, the strength drops almost to zero at temperatures over ~900°C or ~750°C for a "dry" or "wet" upper mantle, respectively [*Ranalli*, 1994; *Burov and Diament*, 1995; *Burov*, 2010].

The rheological parameters used here are given in Table A1. For the sake of simplicity, some parameters are taken as uniform (e.g., strain rate, pore fluid factor, and mantle rheology), representing the "average conditions" that likely approach the "real conditions" of the study area. The increase of the pore fluid factor (to simulate the presence of superhydrostatic pressures) from the value 0.4, chosen in this study, to 0.6 and 0.8 may lead to a decrease of the integrated strength by 25% and 50%, respectively [*Tesauro et al*., 2010]. Since the strain rate is uncertain, we use an average constant value (10^{-15} s^{-1}) to avoid introducing an unnecessary free parameter. However, it should be noted that the strain rates may be higher (or lower) by one or two orders of magnitude in the tectonically active (or stable) areas, respectively [e.g., *Kreemer et al*., 2014]. For this reason, we also calculate integrated strength using strain rates of 10^{-14} s^{-1} and 10^{-16} s^{-1} (see supporting information).

The density of the crustal layers is estimated by the conversion of the seismic velocities [*Tesauro et al*., 2014b] using experimentally determined relationships [*Christensen and Mooney*, 1995]. The density of the sediments has been estimated by *Mooney and Kaban* [2010] who constructing density-depth relationships for each specific basin based on averaged borehole data, depth-dependent compaction relations, and seismic profiling data. The density of the upper mantle, estimated by *Tesauro et al*. [2014a] depending on temperature and composition, is taken as the average value in the depth range 50–200 km. The density in each lithospheric layer employed in this study varies in a relatively small range (e.g., between 2700 and 2800 kg/m^3 in the upper layer of the crystalline crust), and thus the influence of the uncertainty of the density parameter on the estimated strength and T_e is negligible.

The temperature distribution in the NA upper mantle was estimated in the study of *Tesauro et al*. [2014a] using a joint analysis of the gravity data and two recent seismic tomography models, NA07 [*Bedle and van der Lee*, 2009] and SL2013sv [*Schaeffer and Lebedev*, 2013]. The seismic models are based on similar assumptions and data, since both of them were developed using the partitioned waveform inversion technique [*Nolet*, 1990] and utilized, in part, data from the dense distribution of seismic stations provided by the

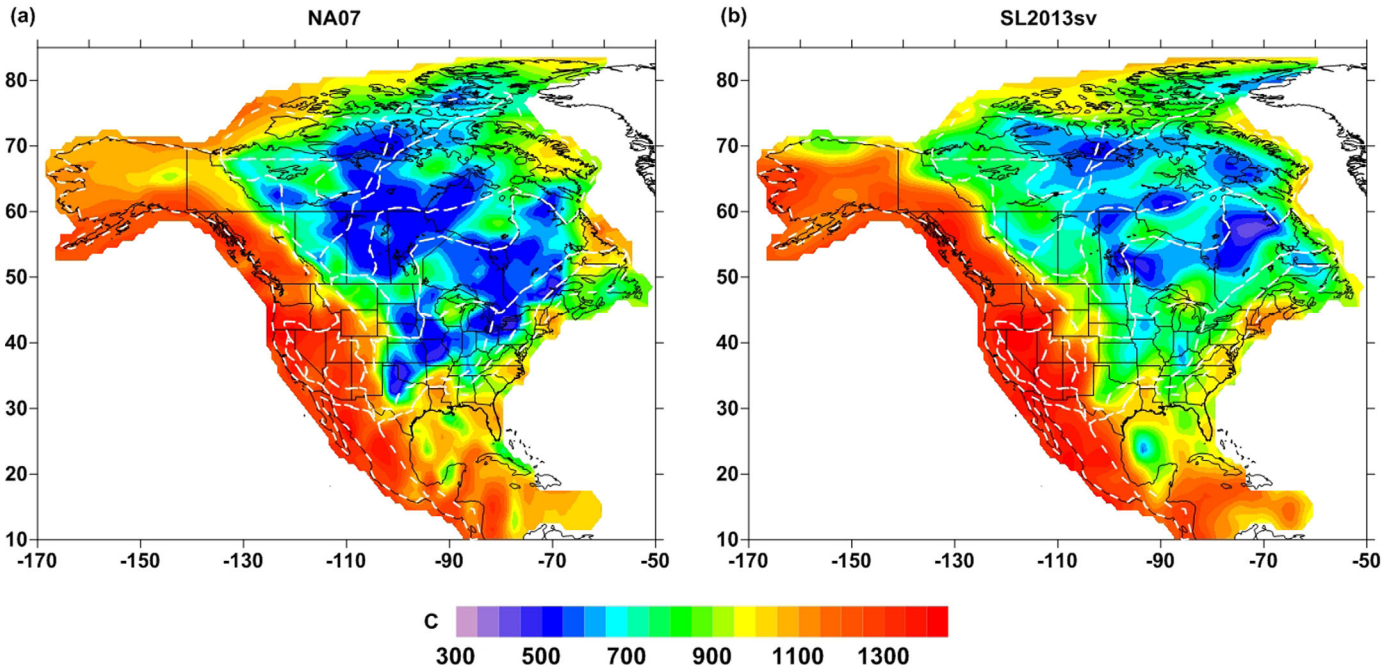

Figure 3. Temperatures (°C) in the NA upper mantle, at 100 km depth [*Tesauro et al*., 2014a], estimated from joint inversion of gravity data and (a) the regional tomography model NA07 [*Bedle and van der Lee*, 2009] and (b) the global tomography model SL2013sv [*Schaeffer and Lebedev*, 2013]. White-dashed contours show the boundaries between tectonic provinces as in Figure 1. See text for further explanation.

USArray. The method used to estimate lithospheric temperatures involved a joint inversion that yields 3-D lithospheric density model that considers the effects of both thermal and compositional variations in the upper mantle [*Kaban et al*., 2014]. This model is based on the residual mantle gravity anomalies and residual topography, which were estimated by subtracting the effects of the crust from the observed fields. The two tomographic models were initially converted to temperatures using mineral physics equations [e.g., *Stixrude and Lithgow-Bertelloni*, 2005]. In the first step, a uniform fertile composition and the anelasticity model Q4 of *Cammarano et al*. [2003], which is suitable for a wet Phanerozoic upper mantle, were used. The initial thermal models made it possible to separate to a first order the effects of temperature and composition in the mantle residual gravity anomalies [*Kaban et al*., 2014]. The initial "compositional" density variations are used to estimate the degree of depletion in heavy constituents (CPX, garnet, and *Fe*) in the cratonic areas. Then, all the computations are repeated taking into account the compositional differences. The iterations are repeated until convergence is reached. On account of the compositional correction, the final thermal models (Figures 3a and 3b) show an increase of temperatures in the cratons of up to ∼150°C relative to the initial homogeneous model. In *Kaban et al*. [2014], we used a smooth transition between the final temperature estimated in the cratonic areas and in other parts of the NA continent to prevent the appearance of sharp gradients, which could be artificial. Possible sharp temperature changes are related to seismic tomography anomalies, which are translated into the temperature model. In turn, the compositional model used in the inversion controls average absolute temperatures. The estimated lithospheric temperatures were extrapolated to the surface using typical geotherms determined for different tectonic provinces on the basis of heat flow data [*Hasterok and Chapman*, 2011; *Currie and Hyndman*, 2006].

Both thermal models, named according to the corresponding tomography models (NA07 and SL2013sv), show a significant temperature difference of up to ∼700°C at a depth of 100 km between the internal part and the western portion of the continent (Figures 3a and 3b). The high temperatures beneath the NA Cordillera are in agreement with the high surface heat flow [e.g., *Blackwell and Richards*, 2004] and low resistivity [e.g., *Rippe et al*., 2013] and reflect the presence of aqueous fluids associated with past subduction [*Hyndman and Currie*, 2011] and a melt fraction of up to 1.5% in the shallow upper mantle [*Rippe et al*., 2013].

The coldest lithosphere in both models underlies the Archean Churchill, Slave, and Superior cratons and, for the model NA07, parts of the Proterozoic terranes (e.g., Trans-Hudson Orogen). These results are generally

well within the range of the geotherms estimated from xenolith data [e.g., *Griffin et al.*, 2003; *Pollack and Chapman*, 1977; *Hasterok and Chapman*, 2011]. In particular, in the Archean cratons at a depth of 100 km the estimates provided by the NA07 model are close to the lower boundary of the range defined by xenolith data (~600°C), while those of SL2013sv model fall in the middle (~750°C). The models show relatively large differences within some Proterozoic regions, such as the Grenville and Yavapai-Mazatzal province (Figures 3a and 3b), where the NA07 model predicts values lower (by ~200°C) than those of the SL2013sv model.

Lou and van der Lee [2014] report a larger delay time contrast across the Appalachians than the Grenville province, indicating that the lithosphere of the North American Craton extends at least to the Appalachians. Therefore, the difference in temperatures between the models NA07 and SL2013sv, which tends to be reduced at larger depths, is probably related to the different resolution of the tomography models at the edge of the NA craton. On the other hand, in both models some peripheral parts of the cratons, such as the Archean Wyoming craton and the Proterozoic Colorado Plateau, are characterized by a hot upper mantle (Figures 3a and 3b). Xenolith data indicate that the high temperatures beneath the Wyoming Craton are due to Phanerozoic mantle refertilization. *Carlson et al*. [2004] infer a prolonged history of lithospheric melting within the uppermost part of the lithospheric mantle. The upper mantle of the Colorado Plateau was probably heated during the last 30–40 My, as a consequence either of the Farallon slab roll-back [*Roy et al*., 2009] or asthenospheric upwelling that progressively infiltrated and modified the lithosphere [e.g., *Schmandt and Humphreys*, 2010; *Crow et al*., 2011].

Although the two thermal models take into account the effect of compositional variations and anelasticity, they are affected by uncertainties, mainly depending on those of the seismic tomographic models. An uncertainty of the *S* wave velocity of the tomography model of ~0.05 km/s translates into errors in estimates of temperature up to ~150°C in cold cratons [*Tesauro et al*., 2012a]. The effect is significantly smaller in hot areas, where velocity variations correspond to smaller temperature changes due to anelasticity. The largest uncertainties of the elastic parameters are their temperature derivatives (with 10% and 20% uncertainties) [e.g., *Cammarano et al*., 2003], leading to an uncertainty in the inferred temperatures of about ~70°C above 300 km [*Tesauro et al*., 2010]. The uncertainties of the anelasticity model might be large at high temperatures [e.g., *Cammarano et al*., 2003]. However, they do not affect the strength estimates, since the anelasticity starts to be activated at temperatures exceeding 900°C [e.g., *Jackson*, 2002] when the strength is already close to zero.

3. Strength Variations in the NA Lithosphere

Using the rheology and the two thermal models described above, the integrated strength of the lithosphere (σ_L) under compression through integration of the yield strength envelope (YSE) is estimated according to:

$$\sigma_L = \int_0^h (\sigma_1 - \sigma_3) \cdot dz \tag{1}$$

where h is the thickness of the lithosphere and z is the depth.

In both models, here named as the corresponding tomography and thermal models, the integrated lithospheric strength (Figures 4a and 4b), shows significant spatial variations. The largest values ($>1 \times 10^{14}$ Pa m) correspond to the Archean and Proterozoic cratons, while in the Phanerozoic lithosphere the integrated strength is reduced to values $<1 \times 10^{13}$ Pa m. Such a sharp variation occurs in the model NA07 beneath the Rocky Mountains, the eastern border of the Canadian Cordillera and the southern border of Grenville province. In the model SL2013sv, the transition from strong to weaker lithosphere is shifted more to the east, crossing the Yavapai-Mazatzal province, the Trans-Hudson Orogen (THO) and the Proterozoic Canadian platform, and to the north, crossing the northern border of Grenville province (Figures 4a and 4b). Consequently, the regions characterized by a strong lithosphere in the model SL2013sv cover significantly less area than in the model NA07, since they do not include the peripheral cratonic regions. The lithospheric strength is 10 times larger there in the model NA07 than in the model SL2013sv (Figures 4a and 4b), on account of the difference in temperatures exceeding 200°C (Figures 3a and 3b). The strength profiles representative of these regions show that the difference in temperature influences mostly the strength of the mantle lithosphere, which is close to zero in the model SL2013sv, while in the model NA07 its brittle part has a thickness >30 km in the western part of the Yavapai-Mazatzal province (Figure 5a) and over 50 km in

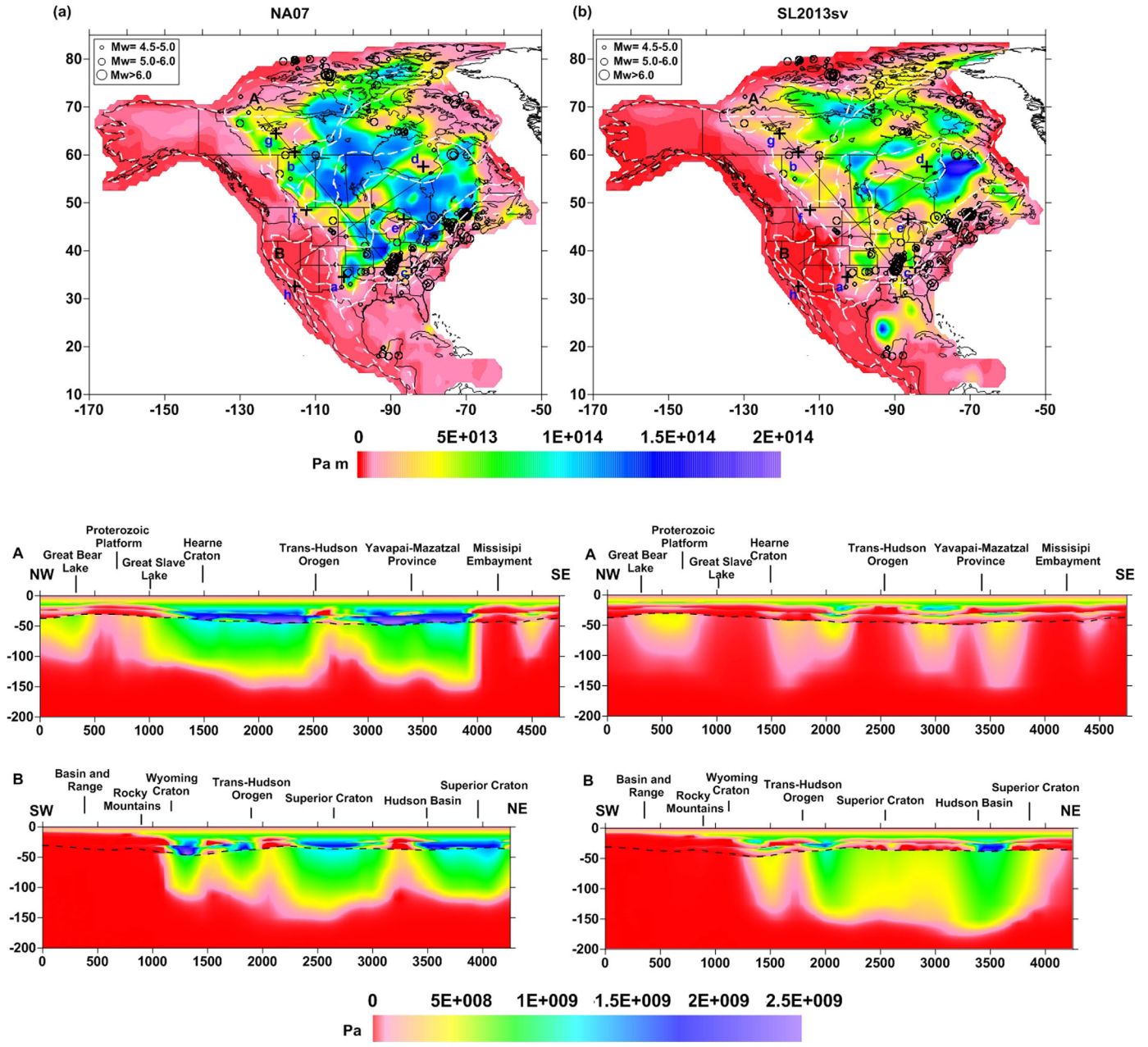

Figure 4. Integrated lithospheric strength (Pa m) and strength distribution (Pa) along two cross sections estimated in compression using the crustal rheological types (Figure 2) and (a) the NA07 thermal model (Figure 3a); (b) the SL2013sv thermal model (Figure 3b). White-dashed contours show the boundaries between the tectonic provinces as in Figure 1. Black circles show intraplate earthquakes location belonging to the seismic catalog for stable continental regions (SRCs) of *Schulte and Mooney* [2005]. Black lines with capital letters show the locations of the cross sections. Black crosses with blue letters show the locations of the YSEs displayed in Figures 5a–5h. See text for further explanation.

the Proterozoic Canadian Platform (Great Slave Lake) (Figure 5b). The large difference in the lithospheric mantle strength between the two models in the westernmost part of the craton is also visible from cross-section A, Figures 4a and 4b. Due to the difference in temperatures, in model NA07 the lithospheric mantle retains significant strength ($>5 \times 10^8$ Pa) on average up to a depth of 100 km in all tectonic provinces except for the southwestern border of the craton (Mississippi Embayment and surroundings). In contrast, in SL2013sv the lithospheric mantle is relatively strong up to shallower depths (~70 km) and only in some parts of the western edge of the NA craton.

Other peripheral parts of the cratons, such as the southern border of the Proterozoic craton, the Wyoming craton and the Colorado Plateau, have in both models a weak lithosphere with the strength prevalently

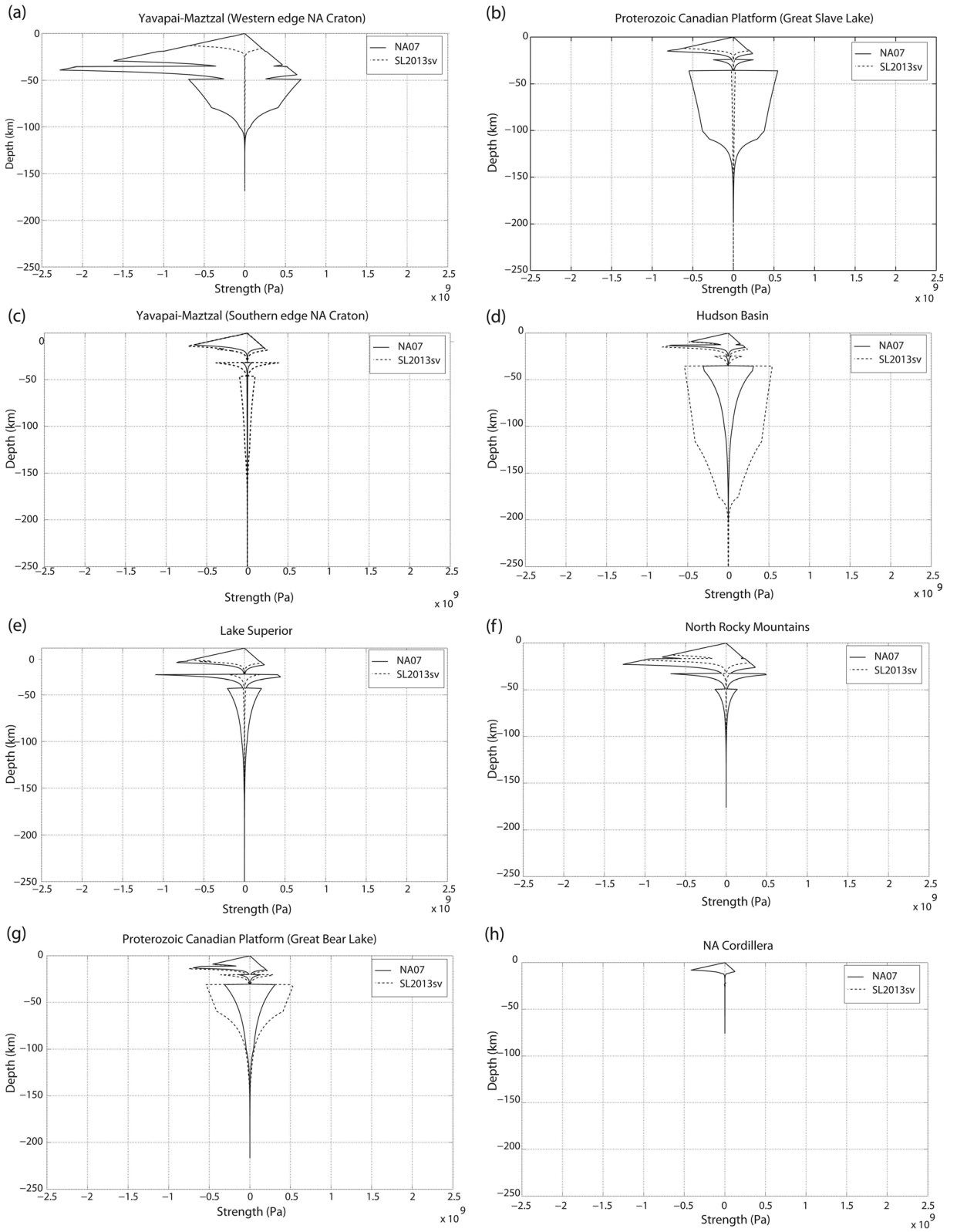

Figure 5. YSEs estimated using as input the NA07 thermal model (continuous black lines) and SL2013sv thermal model (dashed black lines) in different tectonic province of NA continent. For convention, the values estimated under compressional and extensional conditions are shown as negative and positive, respectively. Location of the strength profiles is displayed in Figures 4a and 4b. See text for further explanation.

limited to the crust (Figures 4a, 4b, cross-section B; Figure 5c), on account of their hot upper mantle (Figures 3a and 3b). In contrast to the global models, where the areas of high strength corresponding to the cratons extend up to the continental margins [*Tesauro et al*., 2013], in both models NA07 and SL2013sv the continental margins and the Appalachians are characterized by a weak lithosphere (Figures 4a and 4b). In other regions off-cratons, such as the Gulf of Mexico, the two models show different results, with the lithosphere significantly stronger in the model SL2013sv than in NA07 (Figures 4a and 4b), on account of the lower temperatures (Figures 3a and 3b).

In the inner part of the cratons, as in the Superior craton and Hudson basin, the strength in the lithospheric mantle is doubled in the model SL2013sv in comparison with NA07, on account of the lower temperatures (Figures 3a and 3b). In this area, the brittle layer of the lithospheric mantle reaches values over 50 km in the model SL2013sv, while in the model NA07 it is only few km thick (Figure 5d). From cross-section B in Figures 4a and 4b, we can observe that in the model NA07 the lithospheric mantle of the cratons is stronger than in the model SL2013sv in its shallowest part, but the model NA07 becomes weaker than the model SL2013sv below a depth of $\sim$120 km. Both NA07 and SL2013sv show local weakness within the cratonic lithosphere beneath the intracratonic Illinois Basin and Midcontinent rift (Figures 4a and 4b) where the mantle lithosphere has no brittle strength (Figure 5e). Such a local weakness might be explained by the presence in the shallow mantle of an unusual crust-mantle mixture [*Bedle and van der Lee*, 2006].

The strength in the crust shows a similar distribution as the strength in the lithosphere (Figures 6a and 6b), indicating that the temperature variations have a greater influence on strength than crustal composition. The absence of a direct correlation between crustal composition and strength variations can be particularly noticed in the northern part of the Rocky Mountains, where both models indicate a weak crust and subcrustal lithosphere (Figures 4a, 4b, 6a, 6b, and 5f), even with the "hard" rheology (Figure 2 and Table 1). In general, the largest values of lithospheric and crustal strength correspond in both models to the coldest areas with thick crust, while the lowest values correspond to the warmest areas, despite the rheology assumed (Figures 6a and 6b). Indeed, in the entire NA Cordillera the strength, located prevalently ($>$90%) in the crust in both models (Figures 4a, 4b, cross-section B; Figures 6c and 6d), is strongly reduced (Figure 5h), despite the fact that the Columbia Plateau and the Canadian Cordillera have a stronger crustal rheology in comparison with that of the Basin and Range (Figure 2 and Table 1). These results, similar to those provided by the global strength models [*Tesauro et al*., 2012a, 2013], reflect the repeated weakening of the young terrains of the continental margins by thermal rejuvenation and fault reactivation during subduction, orogeny, and rifting, whereas the continental cores were left mostly undeformed and thermally stable. In contrast to Phanerozoic crust, in cratonic regions $\sim$40% of the strength is localized in the crust in the model NA07, while in the model SL2013 the percentage decreases up to $<$15% in the northern part of the Canadian Shield (Figures 6c and 6d). In these areas, the thermal model SL2013sv has a smoother temperature gradient than the model NA07 [*Tesauro et al*., 2014a], making the lithospheric mantle colder and stronger (Figures 7a and 7b). Hence, compositional variations within the crust influence the integrated crustal strength only if the thermal regime is intermediate. In fact, in the model NA07 the western part of the Yavapai-Mazatzal province and the Proterozoic Canadian Platform (Great Bear Lake) are both characterized by relatively low temperatures (Figure 3a), but the crust of the former region retains more strength than the crust of the latter (Figures 4a and 4b, cross-section A; Figures 5a and 5g), on account of its stiffer rheology and thick crust (Figure 2 and Table 1). In contrast, the lithospheric mantle shows similar thickness of its brittle layer (Figures 5a and 5g).

We can also observe that there is no correlation between the integrated strength distribution in the crust and its thickness [*Tesauro et al*., 2014b]. Indeed, although the NA Cordillera has a variable crustal thickness, from 40 to 45 km in the Columbia Plateau to $<$30 km in the Basin and Range, the integrated strength is very low, on account of the high temperature in this region. On the other hand, the thinning of the crust from the Superior craton and the THO toward the northern part of the Canadian Shield (from $\sim$45 to $\sim$30 km) [*Tesauro et al*., 2014b] leads to a concentration of strength in the mantle lithosphere in this area that is characterized by low mantle temperatures (Figures 6c and 6d).

Varying the strain rate by one order does not change significantly the distribution of the integrated lithospheric and crustal strength (supporting information Figures S1 and S2). Indeed, even if the North American Cordillera, being a tectonically active region, is likely characterized by strain rates that are larger than cratonic areas [e.g., *Kreemer et al*., 2014], its integrated strength remains low on account of high temperatures. In contrast, in the cratonic areas, which are tectonically stable, the strain rates, and thus the integrated

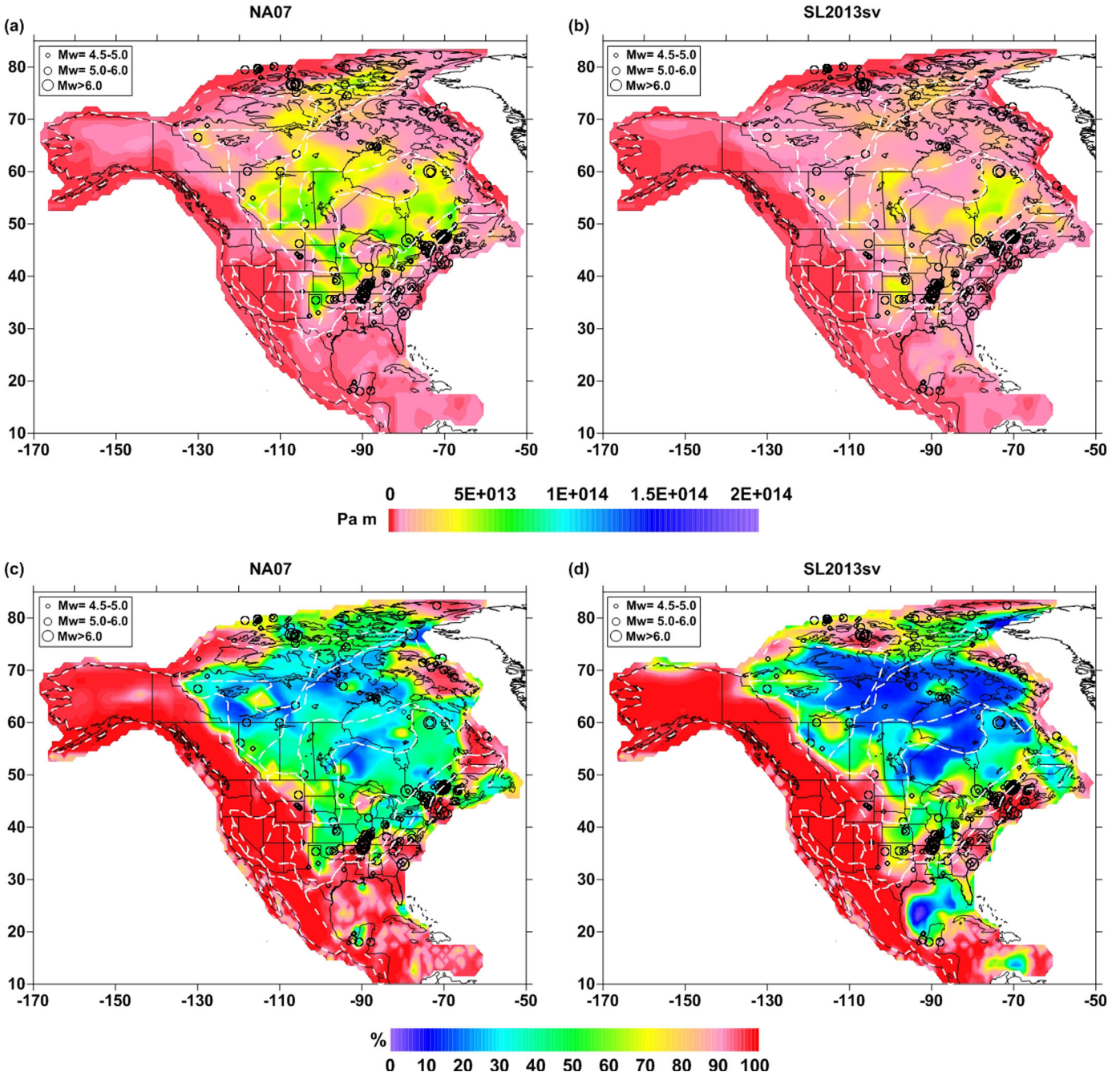

Figure 6. Integrated crustal strength (Pa m) in compression and fraction (%) of the integrated total strength contributed by the crust estimated using the crustal rheological types (Figure 2 and Table 1) and (a and c) the thermal model NA07 (Figure 3a); (b and d) the thermal model SL2013sv (Figure 3b). White-dashed contours show the boundaries between the tectonic provinces as in Figure 1. Black circles show intraplate earthquakes location from the seismic catalog for stable continental regions (SRCs) of *Schulte and Mooney* [2005]. See text for further explanation.

strength, may be lower than the value assumed in this study. However, also in this case, the difference in the integrated strength between the cratonic and off-cratonic regions is remarkable (supporting information Figures S1 and S2). In addition, we can observe that the effective viscosity (η) of the crust and mantle lithosphere estimated along two cross sections for the strain rates in the range 10^{-14} to 10^{-16} s^{-1} shows significant variations only within the cratons (between 10^{22} and 10^{25} Pa s) (supporting information Figures S3 and S4). In contrast, in the regions characterized by high temperatures, as the NA Cordillera, η remains below 10^{21} Pa s, indicating a ductile deformation of the lithosphere even when the value of the strain rate is decreased by one order [e.g., *Watts and Zhong*, 2000; *Yaolin and Jianling*, 2008].

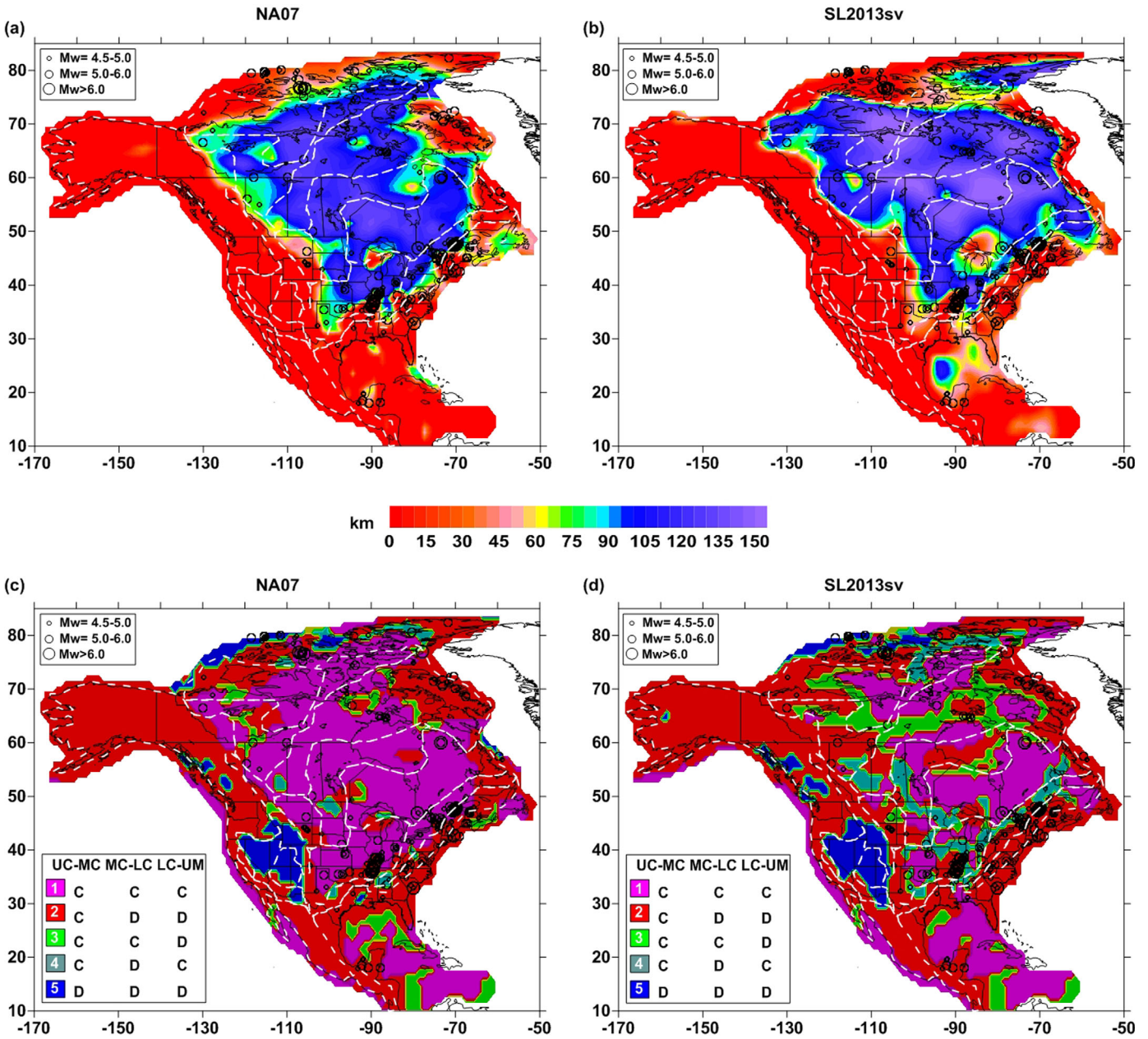

Figure 7. Thickness (km) of the mechanically strong mantle lithospheric (MSML) layer and coupling and decoupling conditions of the lithospheric layers; for (a–c) NA07 and (b–d) SL2013sv. Abbreviations stand as follows: UC, Upper Crust; MC, Middle Crust; LC, Lower Crust; UM, Upper Mantle; C, Coupled conditions; D, Decoupled conditions. In the regions, where the crust is composed of only one or two layers, the condition 3 indicates decoupling of the crust from the mantle lithosphere. White-dashed contours show the boundaries between the tectonic provinces as in Figure 1. Black circles show intraplate earthquakes location from the seismic catalog for stable continental regions (SRCs) of *Schulte and Mooney* [2005]. See text for further explanation.

4. Effective Elastic Thickness of the NA Lithosphere

The effective elastic thickness of the lithosphere corresponds to the thickness of a homogeneous elastic layer, which is characterized by the same flexural rigidity as the lithosphere [e.g., *Burov and Diament*, 1995]. T_e of the continents has a wide range of values (from 5 to over 100 km), which can vary within the plate depending on the coupling-decoupling conditions of the lithospheric layers. When the layers are coupled, T_e generally depends on temperature and is coincident with the base of the mechanical lithosphere, while when the layers are decoupled T_e is significantly reduced (Appendix A). The lithospheric layers (e.g., the lower crust and upper mantle) are decoupled if temperature of the creep activation of the rocks is lower than the temperature at a depth of the boundary layers (Appendix A). In general, if the crust is thicker than

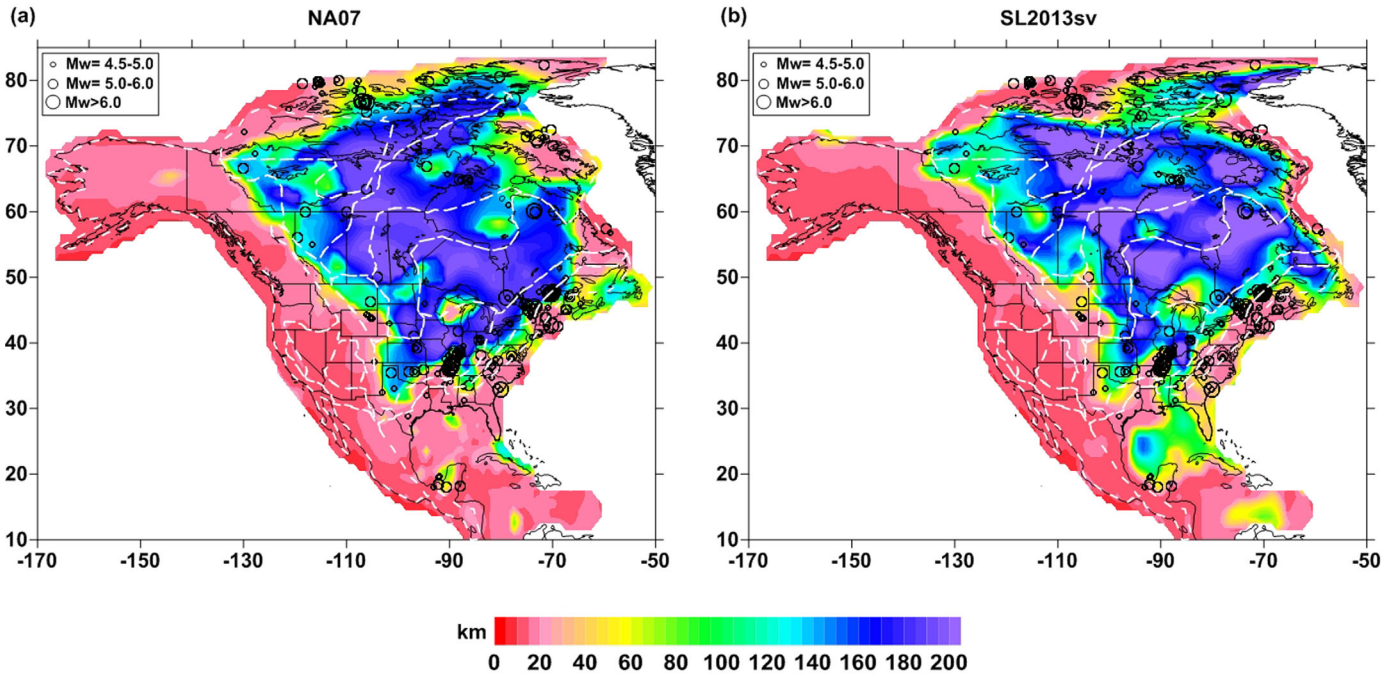

Figure 8. Effective elastic thickness (T_e) of the lithosphere (km) for (a) the model NA07 and (b) the model SL2013sv. White-dashed contours show the boundaries between the tectonic provinces as in Figure 1. Black circles show intraplate earthquakes location belonging to the seismic catalog for stable continental regions (SRCs) of *Schulte and Mooney* [2005]. See text for further explanation.

35 km, the lower-crustal temperatures are high enough to reduce the creep strength of the rocks in the vicinity of the Moho, causing decupling of the crust from the upper mantle [*Burov and Diament*, 1995]. In the opposite case, the crust and mantle are mechanically coupled and the lithosphere behaves like a single plate, similar to the oceanic lithosphere.

The mechanical coupling-decoupling conditions of the NA07 and SL2013sv models (Figures 7c and 7d) are similar in the regions off-cratons. All the lithospheric layers are decoupled beneath the Basin and Range and most of the Colorado Plateau (condition 5 in Figures 7c and 7d; Figures 4a and 4b, cross-section B), while in the other parts of the NA Cordillera and the Appalachians the upper and middle crustal layers are coupled (condition 2 in Figures 7c and 7d). In these young orogenic belts, the thickening of the crust leads to increased temperatures in the lower part of the crust and consequently significantly reduces the strength below the middle crustal depths. This process causes mechanical decoupling between the lithospheric layers and reduces T_e to $<$20 km (Figures 8a and 8b), as a result of the absence of the mechanically strong mantle lithospheric (MSML) layer (Figures 7a and 7b). Other effects, such as reheating and hydration of the lithospheric mantle, occurring in NA Cordillera [e.g., *Hyndman et al*., 2005] and Appalachians [*van der Lee et al*., 2008], associated with the underlying (subducted) Farallon slab, contribute to the decoupling of lithospheric layers. In these regions, characterized by a relatively thick crust and a high thermal regime, a "crème brulee" model [*Jackson*, 2002], in which the mantle is weak and the strength is primarily localized in the uppermost part of the crust (Figures 6c and 6d), is applicable. The lower values of the strength and low T_e ($<$20 km), found in the NA Cordillera, are consistent with the results of previous regional [e.g., *Bechtel et al*., 1990; *Lowry and Smith*, 1995; *Lowry et al*., 2000; *Flück et al*., 2003; *Audet and Mareschal*, 2004b; *Hyndman et al*., 2009; *Kirby and Swain*, 2009; *Lowry and Pérez-Gussinyé*, 2011; *Hardebol et al*., 2013] and global studies [e.g., *Audet and Bürgmann*, 2011; *Tesauro et al*., 2012a, 2013; *Mouthereau et al*., 2013]. Most of the NA Cordillera is characterized by positive residual topography ($>$2 km), which is largely supported by the low-density upper mantle, both within and under the lithosphere [*Becker et al*., 2014; *Kaban et al*., 2014]. The uplift might be related to a hot back arc [e.g., *Hyndman and Currie*, 2011] and/or to an uprising mantle plume (e.g., in Yellowstone, *Parsons et al*. [1994]). However, recent numerical models [*François et al*., 2013] demonstrate that a strong crust alone is insufficient to keep topography stable over significant time. Therefore, the high temperatures of these regions, which is responsible for the 1–2 km elevated topography, reduces significantly their strength and makes them more prone to deformations.

We find a significantly lower value (about 30 km) for T_e in the Appalachians compared with previous studies that estimated an average value of ~50 km [*Armstrong and Watts*, 2001; *Kirby and Swain*, 2009; *Audet and Bürgmann*, 2011; *Mouthereau et al*., 2013]. The low T_e reported here may reflect the presence of a weak upper mantle, possibly due to its hydrated conditions [*van der Lee et al*., 2008]. We find similar difference between our estimates and previous T_e estimates in Alaska. However, the low T_e values (<20 km) are less well constrained in this area due to the lower resolution of the tomography models [*Bedle and van der Lee*, 2009]. On the other hand, other models of T_e also show conflicting results. Actually, flexural studies [*Mouthereau et al*., 2013] predict T_e values increasing from the southern to the northern part of Alaska (from ~30 to ~50 km), while studies based on cross-spectral analyses of the gravity field [*Kirby and Swain*, 2009; *Audet and Bürgmann*, 2011], reveal an opposite trend. In the off-craton regions, the largest discrepancies between the two T_e models are found, as in case of the strength models, in the Gulf of Mexico, where the values predicted by SL2013sv model are more than the double of those in the NA07 model. However, in this area the lower resolution of the seismic tomography used to estimate the temperatures make the results weakly constrained, and none of the T_e estimates provided by other methods [*Kirby and Swain*, 2009; *Mouthereau et al*., 2013] are robust.

Beneath the cratons the coupling-decoupling conditions are different in the models NA07 and SL2013sv (Figures 7c and 7d). In NA07 most of the Proterozoic and Archean regions have all lithospheric layers coupled (condition 1, Figures 7c and 7d) and the "jelly sandwich" model, in which the strength is distributed within the crust and upper mantle [e.g., *Burov*, 2011], is applicable (Figures 4a and 4b, cross-section B; Figures 6c and 6d). It should be noted that the "classical" jelly sandwich model refers to a rheology with strong upper crust and upper mantle layers, separated by a ductile lower crustal layer that does not allow flexural stresses to be transmitted between layers [e.g., *Afonso and Ranalli*, 2004]. In this study, as in previous studies [e.g., *Burov*, 2010] the definition of "jelly sandwich" model is extended to other variations of the classical model, including the cases in which another crustal layer other than the lower crust is weak or when the entire crust and the upper mantle are strong. Therefore, the main difference with the "crème brulee" model is the presence of a brittle rather than ductile upper mantle.

In the model SL2013sv, the conditions in which all the lithospheric layers are coupled is present only in some parts of the NA cratons, such as the Superior craton, parts of the Churchill and Slave craton and the northern part of the THO (Figures 7c and 7d). Despite the variability of the coupling-decoupling conditions in the model SL2013sv, the "jelly sandwich" model is applicable in most part of the cratons as in NA07, since the strength is partitioned between the crust and the mantle lithosphere (Figures 4a and 4b, cross-section B; Figures 6c and 6d). In the model SL2013sv, the cratonic regions where the strength is prevalently localized in the upper and middle crust, and thus where the "crème brulee" model is applicable, are mostly limited to some peripheral parts (Figures 4a and 4b, cross-section A), as the western part of the Yavapai-Mazatzal province (Figure 5a), parts of the Proterozoic Canadian Platform (Figure 5b) and in the southern edge of the Proterozoic craton (Figure 5c). *Burov* [2010] applied analytical and numerical thermomechanical modeling to evaluate the stability and structural styles associated with various rheological models. His study demonstrated that the "crème brulee" model may be applicable only to some synrift basins, margins and young orogens (e.g., the Basin and Range), while the "classical" "jelly sandwich" model, including its stronger variants, is more typical (intracontinental and old orogens, forelands, shields, and postrift basins) and provides a first-order explanation for the long-term support of the Earth's main surface features. Therefore, according to this study, the weak lithospheric strength of the peripheral cratonic regions estimated in the model SL2013sv should lead to a long time-scale instability of these old (most Proterozoic) geological provinces.

On the other hand, despite the differences between the two models observed in the peripheral part of the cratons, T_e for both models shows large values in most of the cratonic regions (>100 km), significantly deeper than their average crustal thickness (~40 km). These results suggest that high T_e in an old stable craton largely relates to a thick MSML layer (Figures 7a and 7b). In both models, T_e shows similar lateral variations within the cratons (Figures 8a and 8b). In fact, although in the model SL2013sv all the lithospheric layers are coupled only in a limited part of the cratons (Figure 7d), the large strength in the lithospheric mantle (Figures 4a and 4b, cross-section B) and thickness of the MSML layer (Figure 7b) gives T_e similar or larger than in NA07 (Figures 8a and 8b). In this regard, it should be noted that the regions with a relatively weak lithosphere, close to the cratonic edges in the model SL2013sv (Figure 4b) are characterized by large

values of T_e (~100 km) (Figure 8b). Thus, the smooth temperature gradient in the thermal model SL2013sv affects the strength distribution between the lithospheric layers (Figure 6d) and increases the thickness of the MSML layer (Figure 7b), and consequently T_e (Figure 8b). Therefore, the peripheral parts of the cratons, which are weaker in SL2013sv than in NA07 in terms of T_e are mostly limited to the western part of the Yavapai-Mazatzal province and the southern part of the Grenville Province (Figures 8a and 8b). Consequently, most of the cratonic areas are characterized by a long-term stability in both models. In fact, *François et al*. [2013] demonstrated that the strong lithosphere (i.e., $T_e = 100–110$ km) with a MSML layer at least of 60–70 km thick is needed to keep surface and subsurface topographies of tectonic features stable. According to some previous studies [*Kirby and Swain*, 2009; *Mouthereau et al*., 2013], the largest values of T_e (>100 km) are mostly confined to the Archean parts of the NA cratons. The same studies predict T_e values over 50 km for the other parts of the cratons, which implies a relatively strong lithospheric mantle [*Burov*, 2011].

Other studies of the Canadian Shield based on spectral methods [e.g., *Wang and Mareschal*, 1999; *Audet and Mareschal*, 2004a,b, 2007] show T_e values less uniformly distributed than those reported in this study, with variations on short spatial scale (<500 km). However, their inferred spatial pattern is not clearly correlated with either the distribution of the tectonic features or with their age. The T_e values, estimated by *Audet and Mareschal* [2004b] using a multitaper method, are lower than those of *Audet and Mareschal* [2004a], based on the maximum entropy method. However, they show similar trends, with the largest values located in the eastern part of the Hudson basin, and the southern part of the Superior and Hearne craton. In contrast, the estimates of *Audet and Mareschal* [2007] and *Wang and Mareschal* [1999], based on wavelet and maximum entropy method predict large values (>50 km) in most of the Canadian Shield, but with a different distribution. In *Audet and Mareschal* [2007], the largest values (>100 km) are located in the northwestern part of the study area, which includes the Hudson basin, the northern part of the THO and the Rae craton, while *Wang and Mareschal* [1999] found maximum values for T_e in the northern part of THO and central part of the Superior craton. Notably, *Poudjom Djomani et al*. [2005] have detected in the Slave craton a correlation between T_e and mantle composition, estimating large values (>50 km) in the younger eastern part of the craton, which is separated from the older western part by a zone of steep T_e gradients parallel to the major locus of kimberlite intrusions. The T_e values estimated in this study do not show such a correlation, being the entire Slave craton characterized by high T_e values (Figures 8a and 8b).

We further notice that in both NA07 and SL2013sv T_e estimates vary sharply at the boundaries of the cratons due to the corresponding abrupt change of the thickness of the MSML layer (Figures 7a and 7b). Such a feature has been also observed in previous studies based on a rheological approach [*Hyndman et al*., 2009; *Hardebol et al*., 2013] and on the free-air gravity/topography (i.e., admittance), calculated using wavelet transforms [*Kirby and Swain*, 2014]. In contrast, the studies based on other methods [*Wang and Mareschal*, 1999; *Flück et al*., 2003; *Kirby and Swain*, 2009; *Audet and Mareschal*, 2004; *Audet and Bürgmann*, 2011; *Mouthereau et al*., 2013] show a much smoother transition in the peripheral parts of the cratons (Proterozoic regions), which are generally characterized by larger and lower values of T_e (~50 km) in comparison with those predicted by the NA07 and SL2013sv model, respectively. In addition, T_e values may have a stronger variability in these areas with respect to those estimated in our and similar studies. Indeed, the edges of the cratons, having been deformed during the accretion of the Phanerozoic belts [*Karlstrom, and Humphreys*, 1998], may be affected by local variations of the strain rates [e.g., *Gueydan et al*., 2014] not considered in the models of T_e.

We note that estimates of T_e have larger uncertainties than estimates of strength. Indeed, the thickness of MSML layer depends on the assumption used to define the lower boundary of this layer. As specified in section 2, the thickness of what are considered as "strong" lithospheric layers extends from the top of the layers (in this case the upper mantle) to the depth at which the yield stress is less than some predefined value. Therefore, the choice of this value directly influences T_e, determining also the coupling-decoupling conditions.

5. Strength and Intraplate Earthquakes Distribution

In this section, we compare variations of the lithospheric strength and T_e with distribution of the intraplate earthquakes. Intracrustal seismicity is a result of brittle failure of the lithospheric plate and thus there may

be a correlation between the earthquakes distribution and lateral lithospheric strength variations. We use the global seismic catalog for stable continental regions (SRCs) of *Schulte and Mooney* [2005] updated up to July 2012. The catalog includes 1629 crustal earthquakes with moment magnitudes (Mw) >4.5, of which 238 are located in the study area (Figures 4a and 4b). Instrumental [*Engdahl and Villasenor*, 2002] and historical earthquakes [*Triep and Sykes*, 1996; *Johnston et al*., 1994], for which the Mw has been assigned based on the methodology described by *Johnston* [1989], are included in the catalog. The majority (~70%) of the intraplate earthquakes have Mw < 5.0, while the strongest events (Mw > 6.0) represent only a small part (~6%).

There exists a high concentration of seismicity along the northeastern and southeastern edges of the cratons and in particular in the New Madrid Seismic Zone, the area underlying a Precambrian rift that may have been reactivated during the opening of the Atlantic Ocean [e.g., *Kane et al*., 1981]. This region is characterized by a weak lithosphere in both strength models, on account of relatively high temperatures (Figures 4a, 4b, 8a, and 8b). A correlation between seismicity and cratonic edges is reported for the Siberian and Congo craton [*Craig et al*., 2011; *Sloan et al*., 2011], whereas *Mazzotti* [2007] observed a concentration of seismicity in eastern North America at the edge of the NA craton. *Mooney et al*. [2012] showed that a high proportion of these intraplate events are concentrated in the zones of sharp lateral variations in the lithospheric thickness at the edge of the cratons. In contrast, the Archean and Early Proterozoic cratons have fewer crustal earthquakes and a lower maximum earthquake catalog moment magnitude.

Since significant lateral variations of the lithospheric thickness correlate with the corresponding change in the integrated lithospheric strength, we check a possible correlation between the locations of the intraplate earthquakes and the edges of the cratons by plotting the percentages of the number of the intraplate earthquakes versus the total, mantle lithospheric, and crustal integrated strength for both models (Figures 9a and 9b). The percentages of the seismic events are also plotted versus T_e estimated in the two models (Figure 9c). Indeed, *Audet and Bürgmann* [2011] argue that the magnitude and spatial variations of T_e control the degree, style, and location of deformation in response to long-term tectonic loads, and potentially the distribution of seismic activity. In addition, *Lowry and Smith* [1995] observed that the seismicity along the Intermountain Seismic Belt of the NA Cordillera occurs in a zone of transition from low to high T_e.

Despite the differences in the integrated strength between the two models in the peripheral parts of the cratons (Figures 4a and 4b), the histograms show similar trends (Figures 9a and 9b). In both cases, a large percentage of the seismic events occurs in the areas characterized by a weak lithosphere, in which the strength is mainly localized in the crust and reduced to the values of $\sim 0.5 \times 10^{13}$ Pa s or even less. The percentage of the earthquakes occurring in the regions with relatively high strength ($>1.5 \times 10^{13}$) Pa s is larger in model NA07 (37%) than in model SL2013sv (23%). In model NA07, the intraplate earthquakes are almost equally distributed (~40% in each region) between the regions with low (<30 km) and high values (>100 km) of T_e. In contrast, in the model SL2013sv about 50% of the events are located in the regions with low T_e, while a lower percentage (32%) occurs in the areas where T_e is high (Figure 9c). These results indicate that a relatively large number of intraplate earthquakes occur in the areas characterized by a strong lateral variation of the integrated strength and T_e.

The higher concentration of seismicity in the regions which should resist deformation in the model NA07 compared with SL2013sv may be explained by some overestimation of the integrated strength and T_e. This hypothesis cannot be proved, since the upper bounds of the integrated strength and T_e, over which the brittle failure of the lithosphere becomes unlikely, cannot be defined. On the other hand, the strength model NA07 might be reliable as well, since it correlates better than the model SL2013sv with the intraplate seismicity in the areas characterized by steep changes of strength and T_e, already observed in previous studies [e.g., *Jiménez-Díaz et al*., 2014]. These variations occur in the crust and extend down to the upper mantle.

Since the seismic moment (M_0) better represents the total earthquake energy $\left(Mw = \frac{2}{3}\log\left(M_0\right) - 6.0\right)$, we plot the sum of the seismic moment of the intraplate earthquakes versus the integrated strength and T_e (Figures 10a–10c). We can observe that despite the relatively high number of earthquakes occurring in the regions with high strength and T_e, the largest values of the sum of the seismic moment correspond in both

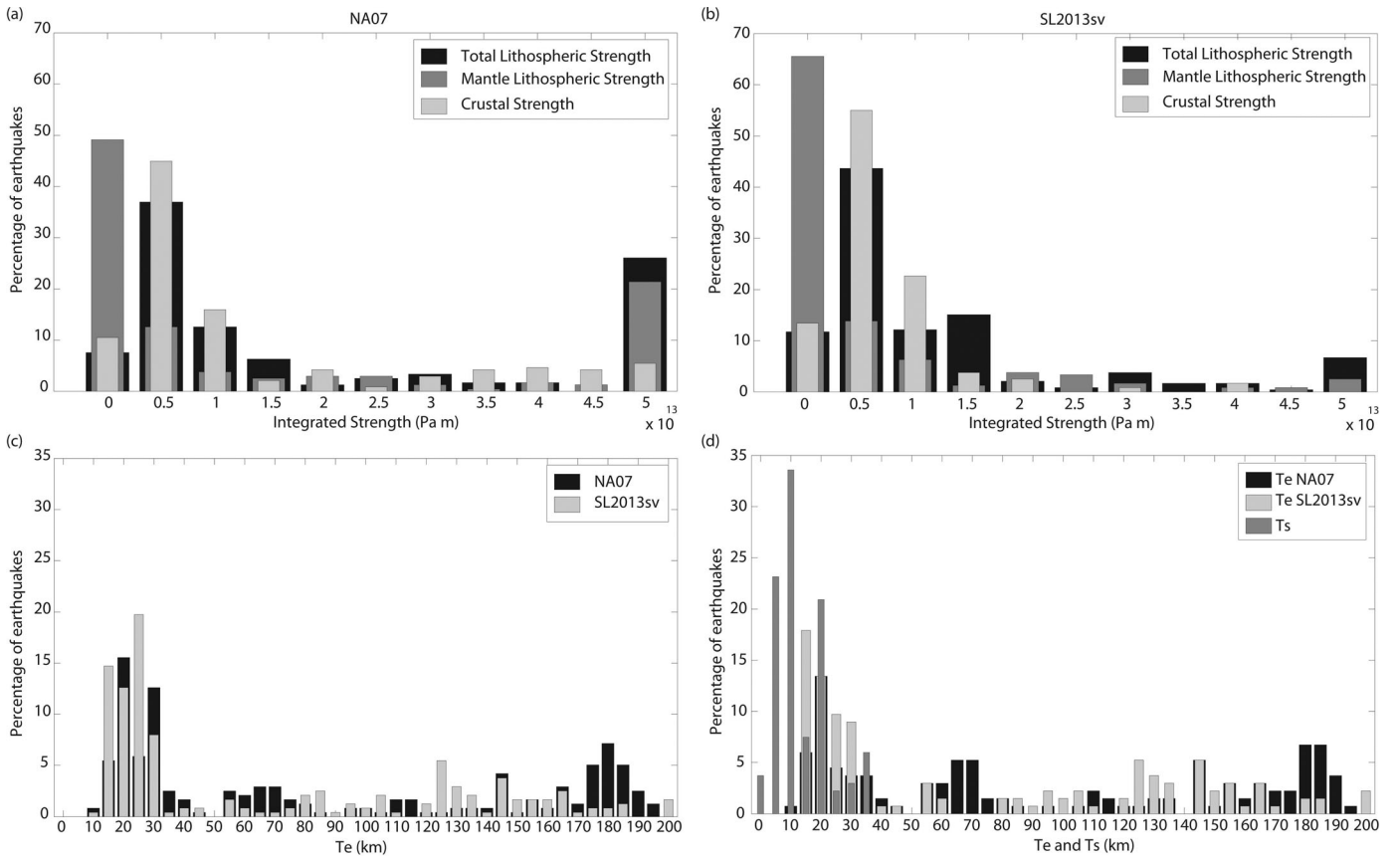

Figure 9. Histograms of the percentage of the number of North American intraplate earthquakes, belonging to the seismic catalog for stable continental regions (SRCs), *Schulte and Mooney* [2005], versus (a and b) the integrated strength of the lithosphere (in black), lithospheric mantle (in dark gray) and crust (in light gray), for (a) the model NA07 and (b) the model SL2013sv; (c) the effective elastic thickness (T_e) for the strength models NA07 (in black) and SL2013sv (in light gray) (d) the effective elastic thickness (T_e) for the same strength models (in black and light gray as before) estimated in the points where the depth of the intraplate earthquakes was evaluated and the seismogenic thickness (Ts) (in dark gray). See text for further explanation.

models to low values of the integrated strength ($<1 \times 10^{13}$ Pa m) and T_e (<30 km). These results demonstrate that seismic energy is mostly released within the weak lithosphere.

Intraplate seismicity is usually concentrated in a specific depth interval called the seismogenic layer (T_s), which is commonly 15–20 thick km and rarely exceeds 40–50 km either in oceanic or continental lithosphere [e.g., *Wiens and Stein*, 1983; *Maggi et al*., 2000]. Some authors suggest that T_s is related to the long-term lithospheric strength, and thus to T_e [*Maggi et al*., 2000; *Jackson*, 2002; *McKenzie and Fairhead*, 1997]. For this reason, they hypothesized that the two parameters are equivalent, implying that the strength of the lithosphere resides only in the crust ("crème-brulee" rheology model). More recent studies demonstrated that T_s and T_e do not necessarily correspond to the same layer in the lithosphere [e.g., *Burov and Watts*, 2006]. These parameters might be equal only when related to the flexural deformation of the lithosphere, when the plate comprises equally strong brittle and ductile parts.

The depth of the intraplate earthquakes, occurring in the area of study, was estimated for only 167 events. The majority of them (~85%) occur in the upper and middle crust (55% at a depth <10 km and 30% at a depth between 10 and 20 km, Figure 9d), where the two layers are coupled (Figures 7c and 7d). The remaining seismic events are located in the lower crust, where the temperatures are usually higher (up to ~600°C) than the normal maximum crustal temperature at which intraplate seismicity occurs (~350°C). Seismicity in the lower crust could be explained by the rheology equivalent to that of the anhydrous granulite-facies material, similar to that assigned (Figure 2 and Table 1). Such a rheology, being metastable under typical lower crustal conditions, rapidly undergoes conversion to weaker eclogites upon the addition of small amounts of water [e.g., *Craig et al*., 2011; *Sloan et al*., 2011], and thus is characterized by brittle deformations at relatively high temperatures.

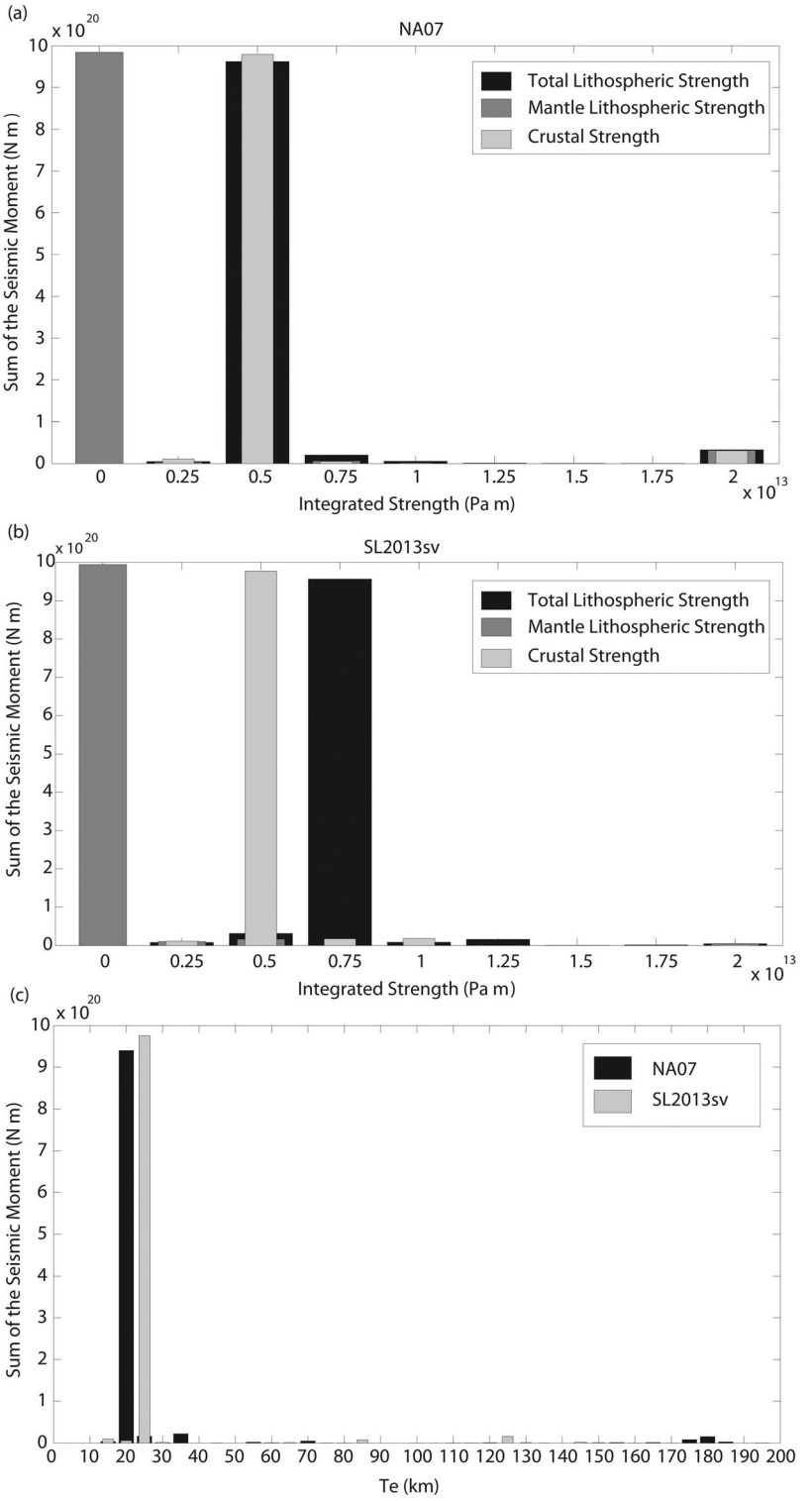

Figure 10. Histograms of the sum of the seismic moment (N m) of North American intraplate earthquakes, belonging to the seismic catalog for stable continental regions (SRCs), *Schulte and Mooney* [2005], versus (a and b) the integrated strength of the lithosphere (in black), lithospheric mantle (in dark gray), and crust (in light gray), for (a) the NA07 model and (b) the SL2013sv model; (c) the effective elastic thickness (T_e) for the strength models NA07 (in black) and SL2013sv (in light gray). See text for further explanation.

There is a large difference between T_e estimated from the strength models NA07 and SL2013sv and the depth of the intraplate earthquakes (seismogenic thickness, T_s). T_e is higher in the model NA07 in most of cases (on average ~80 km in NA07 versus ~60 km in SL2013sv) (Figure 9d). In fact, T_e reflects the response of the lithosphere to long-term geological loads, while T_s is the thickness of the uppermost weak layer that responds on historical time scales to stresses by faulting and earthquakes [e.g., *Watts and Burov*, 2003; *Handy and Brun*, 2004].

6. Conclusions

We evaluate the effects that temperature variations and structure of the lithosphere have on the strength and effective elastic thickness (T_e) of North America using two thermal models. These models are obtained by the joint inversion of gravity data [*Kaban et al*., 2014] and two seismic tomography models [NA07, *Bedle and van der Lee*, 2009; and SL2013sv, *Schaeffer and Lebedev*, 2013]. We have also applied a correction for the effects of compositional variations and anelasticity [*Tesauro et al*., 2014a]. Different types of crustal rheology are assigned using the velocity variations estimated in the model NACr14, the most recent North American crustal model [*Tesauro et al*., 2014b]. Several inferences can be made from the two strength and T_e models, identified with the same names of the seismic tomography models NA07and SL2013sv, respectively.

1. The new strength and T_e model of North America, obtained by using the most recent crustal and seismic tomography models, solve small-scale anomalies better than the previous global models [*Tesauro et al*., 2012a, 2013; *Audet and Bürgmann*, 2011; *Mouthereau et al*., 2013]. Both parameters are more heterogeneously distributed within the cratons, revealing localized zones of lithospheric weakness, such as the Illinois basin and Midcontinent rift, and the zones of high strength corresponding to parts of the Archean cratons. In addition, tectonic features neighboring the cratonic edges, such as the Appalachians, are characterized by a relatively weak lithosphere.

2. The integrated lithospheric strength and T_e are more dependent on temperature than on the crustal composition. This fact leads to first-order similarities between the two models, such as the sharp difference in the strength between the cratonic and off-cratons regions. In the Phanerozoic regions the decoupling conditions of the lithospheric layers and the absence of the mechanically strong mantle lithospheric (MSML) layer reduces T_e to values $<$20 km, making the lithosphere behavior like a "crème-brulee" model [*Jackson*, 2002] and thus more prone to instability. In contrast, the inner cold parts of the cratons are the regions with a strong crust and upper mantle and large values of T_e ($>$100 km), where a "jelly sandwich" model is more applicable. Compositional and crustal thickness variations influence the distribution of the crustal strength in the areas characterized by intermediate thermal conditions, as the Proterozoic Canadian Platform and the Yavapai-Mazatzal province.

3. The largest differences between the two strength models NA07 and SL2013sv occur in some peripheral parts of the cratons, such as the Proterozoic Canadian Platform, the Grenville, and the Yavapai-Mazatzal province, where the integrated strength in NA07 is 10 times larger than in SL2013sv, on account of the lower temperatures estimated in the model NA07. Such a difference influences also the strength distribution in the lithospheric layers and consequently the coupling-decoupling conditions in the two models. In the model SL2013sv, in contrast to the model NA07, only some lithospheric layers are coupled, but still the jelly sandwich model is more applicable than the "crème brulee" model in the regions where the mantle lithosphere retains a significant part of the strength.

4. Despite the differences between the lithospheric strength models NA07 and SL2013sv in the peripheral parts of the cratons, T_e shows similar patterns, implying that T_e is relatively unaffected by the uncertainties in the strength. Such a similarity is due to a smoother temperature gradient in the thermal model SL2013sv in comparison with model NA07, which causes large thickness of the MSML layer and consequently of T_e in the former model. Therefore, the absence of the MSML layer, which would cause instability of old tectonic features [e.g., *Burov*, 2010; *François et al*., 2013] is limited in both models to the most deformed part of the NA craton, reactivated during Meso-Cenozoic tectonic episodes (e.g., Rocky Mountains, Colorado Plateau, Wyoming craton, Mississippi Embayment). Previous estimates of T_e based on flexural studies and inverse approaches show intermediate T_e values (~50 km) in these regions, i.e., values between those found in the inner parts of the cratons and the regions off-cratons. Thus, it is often difficult to precisely locate the transition between low and high values of T_e.

5. Comparison of the integrated strength and T_e variations with the distribution of intraplate earthquakes indicates that most of the events occur along the edge of the cratons, in the zones that are characterized by a weak lithosphere or strong lateral variations in integrated lithospheric strength and T_e. The inner, strong parts of the cratons have a very low level of seismicity. In addition, the sum of the seismic moments shows that most of the energy is released in the weak lithosphere close to the cratonic edges. These results suggest that the edges of the cratons are more prone to accumulation of tectonic stress with a subsequent release by earthquakes, in comparison with the stable cratonic regions which resist deformation.
6. Most earthquakes (85%) occur in the uppermost crustal layers (<20 km), while the remaining 15% are located at the depth of the lower crust (<35 km), defining a T_s much thinner than the average T_e (~80 km in NA07 and 60 km in SL2013sv). The deepest events may indicate the presence of a lower crustal rheology equivalent to that of the anhydrous granulite-facies material (similar to that assigned in this study), which can rapidly convert to a weaker eclogite and thus undergo a brittle failure even at relatively high temperatures.

Appendix A: Method Used to Estimate Strength and Effective Elastic Thickness

Strength can be defined as the resistance to deformation, limited by the differential stress required to initiate failure or flow under a given strain rate. Therefore, rock strength may be defined by the deformation mechanism for which, under given conditions, the least amount of differential stress is required. At shallow depths and low temperatures, rocks predominantly deform by brittle mechanisms, generally described by the Byerlee's law [*Byerlee*, 1978].

The principal stress difference ($\Delta\sigma = \sigma 1 - \sigma 3$) at which slip occurs is given by:

$$\Delta\sigma = \alpha\rho g z(1-\lambda) \tag{A1}$$

The tectonic regime coefficient is given by α (taken as 3.0 and 0.75 for compressional and tensile regimes, respectively), λ is the pore fluid factor (ratio of hydrostatic to lithostatic pressure), and ρgz is the overburden pressure.

At greater depths and higher temperatures rocks deform by creep mechanisms that are described by ductile flow laws. The ductile strength depends on rock type and temperature, and also on a grain size (macro and microstructure). In addition, the ductile behavior nonlinearly depends on the strain rate and thus on the time scale of the deformation process. Ductile deformation involves both diffusion creep and various mechanisms of dislocation creep. The first mechanism is dominant at a small grain size and relatively low stresses, which arises for highly sheared material (ductile shear zones) or for very high temperatures. In contrast, at high stresses and moderate temperatures (<1330°C), dislocation creep (2) is dominant.

$$\Delta\sigma = \left[\frac{\dot{\varepsilon}}{A_P}\right]^{\frac{1}{n}} .\exp\left[\frac{E_P}{nRT}\right] \tag{A2}$$

Here $\dot{\varepsilon}$ is the strain rates, A_P the power strain rates, n the power law exponent, E_P the power law activation energy, R, the gas constant, T the absolute temperature. In the upper mantle for stresses exceeding 200 MPa and temperatures between ~400 and ~800°C deformation is controlled by glide of dislocations with lattice resistance or the Peirels stress (i.e., low-temperature plasticity or Dorn law), described by the equation (A3) of *Mei et al*. [2010],

$$\sigma = \sigma_D\left\{1 - \frac{RT}{E_D}\left[2\ln(\sigma) - \ln\left(\frac{\dot{\varepsilon}}{A_D}\right)\right]\right\}^2 \tag{A3}$$

where σ_D is the Plastic law stress, E_D the Plastic law activation energy, and A_D the Plastic law strain rates. For temperatures higher than ~800°C, the deformation is controlled by dislocation creep (A2).

Goetze and Evans [1979] introduced the yield strength envelope (YSE) for the oceanic lithosphere that is a vertical profile that predicts the maximum differential stress supported by rock as a function of depth. The YSE is represented by curves of two different types (Figure A1). At shallow depths the straight line

Table A1. Rheological Model Parameters and Strength Equations

Parameter	Symbol	Units	Sediments	Upper Crust	Middle Crust	Lower Crust	Upper Mantle
Composition				Quartzite (wet)[a]/Quartzite (dry)[a]/Granite(dry)[a]	Diorite (wet)[a]/ Diabase (dry)[a]	Mafic-Ganulite[b]/Diorite (wet)[a]/Diabase (dry)[a]	Olivine PL(dry)[c] Olivine DL(dry)[d]
Density min-max/mean	ρ	km/m^{-3}	1900–2685/2438	2541–2910/2736	2785–2974/2872	2868–3145/2993	3316–3476/3408[e] 3323/3474/3413[f]
Layer thickness min-max/mean	Z	km	0–14/1.7	1.0–29.0/11.2	1–18.0/11.1	1.5–18.0/10.9	10–279/164[e] 10–285/160[f]
Friction coefficient ext/com	F		0.75/3	0.75/3	0.75/3	0.75/3	0.75/3
Pore fluid factor	λ		0.36	0.36	0.36	0.36	0.36
Power law exponent	N			1.9/2.72/3.3	2.4/3.05	4.2/2.4/3.05	3
Power law activation energy	Ep	kJ mol^{-1}		172.6/134/186	212/276	445/212/276	510
Power law strain-rate	A_p	Pa^{-n} s^{-1}		1.26×10^{-13}/ 6.03×10^{-24}/3.16×10^{-26}	1.26×10^{-16}/6.31×10^{-20}/ 6.31×10^{-20}	8.83×10^{22}/1.26×10^{-16}	1.2589×10^{-12}
Dorn law activation energy	E_D	kJ mol^{-1}					320
Dorn law strain-rate	A_D	s^{-1}					1.4×10^{-19}
Dorn law stress	σ_D	Pa					5.9×10^{9}
Strain rate	ε	s^{-1}		10^{-15}	10^{-15}	10^{-15}	10^{-15}
Brittle strength		$\sigma = f\rho g z(1-\lambda)$					
Creep equations							
Power law creep		$\sigma = \left[\frac{\dot{\varepsilon}}{A_P}\right]^{\frac{1}{n}} .\exp\left[\frac{E_P}{nRT}\right]$					
Dorn law creep		$\sigma = \sigma_D\left\{1 - \frac{RT}{E_D}\left[2\ln(\sigma) - \ln\left(\frac{\dot{\varepsilon}}{A_D}\right)\right]\right\}^2$					

[a] *Carter and Tsenn* [1987].
[b] *Wilks and Carter* [1990].
[c] *Karato and Jung* [2003].
[d] *Mei et al.* [2010].
[e] Values refer to the NA07 strength model.
[f] Values refer to the SL2013sv strength model.

corresponding to brittle fracture shows an increase of the strength with depth. At greater depths, the curved line that describes ductile deformation shows that the strength decreases downward exponentially due to the increase of temperature and corresponding decrease of viscosity [*Burov and Diament*, 1995]. The depth at which the brittle and ductile strengths are equal denotes the brittle-ductile transition (BDT), which can be found in the crust and in the uppermost mantle (Figure A1).

From the computed YSE it is possible to define the thickness of the mechanically strong part of the lithospheric layers that extends from the top of the layer to the depth associated to a specific geotherm (e.g., ~350°C for quartzite), at which the yield stress is less than some predefined value [e.g., 10 MPa used in *Ranalli*, 1994]. Therefore, the lithospheric layers are considered decoupled when the strength decreases below this threshold; otherwise the layers are considered coupled. T_e is calculated as the sum of the mechanically strong layer thicknesses (Δh_i) (Figure A1), as described by equation (A4) or (A5), depending on the coupled and decoupled behavior of the layers [*Burov and Diament*, 1995]:

$$T_e^{(n)} = \left(\sum_{i=1}^{n} \Delta h_i^{\,3}\right)^{1/3} \tag{A4}$$

$$T_e^{(n)} = \left(\sum_{i=1}^{n} \Delta h_i\right) \tag{A5}$$

These equations are valid only in case when all layers are characterized by the same Young's modulus (E). T_e, as thickness of the equivalent homogeneous layer with the same flexural rigidity, is usually referred to $E = 100$ GPa. However, the real lithospheric layers are characterized by significantly different values of E. Therefore, we modify the approach of *Burov and Diament* [1995] and re-estimate T_e taking into account depth variations of E [*Tesauro et al.*, 2012b, 2013]. We specify different values of E for each crustal layer (Table 1), as described by equation (A6) [*Behn et al.*, 2002], where E (Pa) is Young's modulus, Vp (m/s), P wave velocity, σ Poisson coefficient, and ρ (kg/m^3) density.

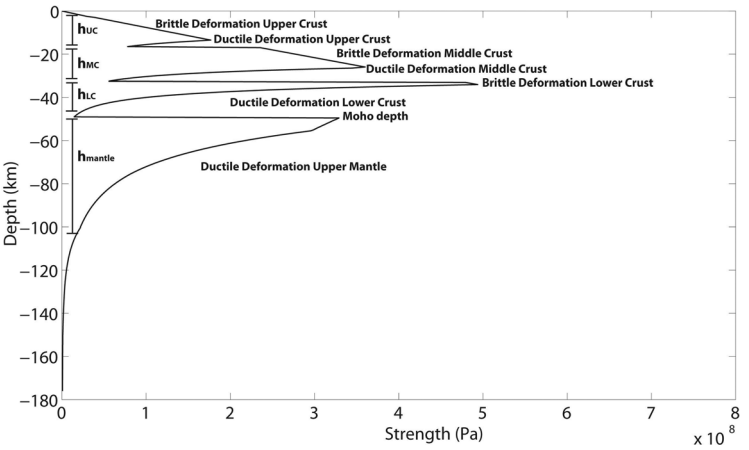

Figure A1. Example of a yield strength envelope (YSE). The abbreviations h_{uc}, h_{mc}, h_{lc}, h_{mantle}, stand as the following: thickness of the mechanically strong part of upper crust, middle crust, lower crust, and upper mantle. See text for further explanation.

$$E = \frac{Vp^2(1+\sigma)(1-2\sigma)\rho}{(1-\sigma)} \tag{A6}$$

The parameters in equation (A6) are defined for each type of crustal rheology (Table 1) following *Christensen* [1996].

The Young's modulus of the lithospheric mantle [*Turcotte and Schubert*, 2014] is twice as large as that of the crust:

$$E = 2G(1+\sigma) \tag{A7}$$

where G (Pa) is the shear modulus.

When E is estimated using the shear modulus of olivine defined for $\sigma = 0.25$ and the P-T range corresponding to brittle conditions, its value is about 180 GPa $\pm$ 10GPa. Since uncertainty of E within the lithospheric mantle is small, we assume an average constant value of 180 GPa.

Acknowledgments
This study was funded by an Alexander von Humboldt Foundation postdoctoral fellowship (M.T.), GeoForschungsZentrum, Potsdam, the USGS National Earthquake Hazards Reduction Program and the Netherlands Research Centre for Integrated Solid Earth (ISES). The data used in this paper are available upon request to the corresponding author. We would like to thank S. Cloetingh for useful discussion, an anonymous reviewer and W. Lewandovski for constructing reviews of an early version of this manuscript.

References

Afonso, J. C., and G. Ranalli (2004), Crustal and mantle strengths in continental lithosphere: Is the jelly sandwich model obsolete?, *Tectonophysics*, *394*, 221–232.
Armstrong, G. D., and A. B. Watts (2001), Spatial variations in *Te* in the southern Appalachians, eastern United States, *J. Geophys. Res.*, *106*, 22,009–22,026.
Artemjev, M. E., and M. K. Kaban (1991), Isostatic processes and intracontinental orogenesis, *J. Geodyn.*, *13*, 77–86, doi:10.1016/0264-3707(91)90031-9.
Audet, P., and R. Bürgmann (2011), Dominant role of tectonic inheritance in supercontinent cycles, *Nat. Geosci.*, *4*, 184–187, doi:10.1038/ngeo1080.
Audet, P., and J. C. Mareschal (2004a), Variations in elastic thickness in the Canadian Shield, *Earth Planet. Sci. Lett.*, *226*, 17–31.
Audet, P., and J.-C. Mareschal (2004b), Anisotropy of the flexural response of the lithosphere in the Canadian Shield, *Geophys. Res. Lett.*, *31*, L20601, doi:10.1029/2004GL021080.
Audet, P., and J. C. Mareschal (2007), Wavelet analysis of the coherence between Bouguer gravity and topography: Application to the elastic thickness anisotropy in the Canadian Shield, *Geophys. J. Int.*, *168*, 287–298.
Audet, P., A. M. Jellinek, and H. Uno (2007), Mechanical controls on the deformation of continents at convergent margins, *Earth Planet. Sci. Lett.*, *264*, 151–166.
Becker, T. W., C. Faccenna, E. D. Humphreys, A. R. Lowry, and M. S. Miller (2014), Static and dynamic support of western United States topography, *Earth Planet. Sci. Lett.*, *402*, 234–246.
Bechtel, T. D., D. W. Forsyth, V. L. Sharpton, and R. A. F. Grieve (1990), Variations in effective elastic thickness of the North American lithosphere, *Nature*, *343*, 636–638.
Bedle, H., and S. van der Lee (2006), Fossil flat-slab subduction beneath the Illinois basin, USA, *Tectonophysics*, *424*(1–2), 53–68.
Bedle, H., and S. van der Lee (2009), *S* velocity variations beneath North America, *J. Geophys. Res.*, *114*, B07308, doi:10.1029/2008JB005949.
Behn, M. D., J. Lin, and M. T. Zuber (2002), Mechanisms of normal fault development at mid-ocean ridges, *J. Geophys. Res.*, *107*(B4), 2083, doi:10.1029/2001JB000503.
Blackwell, D. D., and M. Richards (2004), Geothermal map of North America, sheet 1, scale 1:6,500,000, Am. Assoc. of Pet. Geol., Tulsa, Okla.
Bürgmann, R., and G. Dresen (2008), Rheology of the lower crust and upper mantle: evidence from rock mechanics, geodesy and field observations, *Ann. Rev. Earth Planet. Sci.*, *36*, 531–561.

Burov, E. B. (2010), The equivalent elastic thickness (Te), seismicity and the long-term rheology of continental lithosphere: Time to burn-out "crème brûlée"? Insights from large-scale geodynamic modeling, *Tectonophysics*, *484*, 4–26.
Burov, E. B. (2011), Rheology and strength of the lithosphere, *Mar. Pet. Geol.*, *28*, 1402–1443.
Burov, E. B., and M. Diament (1995), The effective elastic thickness (Te) of continental lithosphere. What does it really means?, *J. Geophys. Res.*, *100*, 3895–3904.
Burov, E. B., and A. B. Watts (2006), The long-term strength of continental lithosphere: Jelly-sandwich or crème-brûlée?, *GSA Today*, *16*, 4–10.
Byerlee, J. D. (1978), Friction of rocks, *Pure Appl. Geophys.*, *116*, 615–626.
Cammarano, F., S. Goes, P. Vacher, and D. Giardini (2003), Inferring upper-mantle temperatures from seismic velocities, *Phys. Earth Planet. Inter.*, *138*, 197–222, doi:10.1016/S00319201(03)00156-0.
Carlson, R. W., I. J. Irving, D. J. Schulze, and B. C. Hearn (2004), Timing of Precambrian melt depletion and Phanerozoic refertilization events in the lithospheric mantle of the Wyoming Craton and adjacent Central Plains Orogen, *Lithos*, *77*, 453–472.
Carter, N. L., and M. C. Tsenn (1987), Flow properties of continental lithosphere, *Tectonophysics*, *136*, 27–63.
Christensen, N. I. (1996), Poisson's ratio and crustal seismology, *J. Geophys. Res.*, *101*, 3139–3156, doi:10.1029/95JB03446.
Christensen, N. I., and W. D. Mooney (1995), Seismic velocity structure and composition of the continental crust: A global review, *J. Geophys. Res.*, *100*, 9761–9788.
Cloetingh, S., and E. Burov (2011), Lithospheric folding and sedimentary basin evolution: A review and analysis of formation mechanisms, *Basin Res.*, *23*, 257–290, doi:10.1111/j.1365-2117.2010.00490.x.
Cloetingh, S., P. A. Ziegler, F. Beekman, P. A. M. Andriessen, L. Matenco, G. Bada, D. Garcia-Castellanos, N. Hardebol, P. Dèzes, and D. Sokoutis (2005), Lithospheric memory state of stress and rheology: Neotectonic controls on Europe's intraplate continental topography, *Quat. Sci. Rev.*, *24*, 241–304.
Clowes, R. M., C. A. Zelt, J. R. Amor, and R. M. Ellis (1995), Lithospheric structure in the southern Canadian Cordillera from a network of seismic refraction lines, *Can. J. Earth Sci.*, *32*, 1485–1513.
Clowes, R. M., D. J. White, and Z. Hajnal (2010), Mantle heterogeneities and their significance: Results from Lithoprobe seismic reflection and refraction/wide-angle reflection studies, *Can. J. Earth Sci.*, *47*, 409–443.
Craig, T. J., J. A. Jackson, K. Priestley, and D. McKenzie (2011), Earthquake distribution patterns in Africa: Their relationship to variations in lithospheric and geological structure, and their rheological implications, *Geophys. J. Int.*, *185*, 403–434.
Crow, R., K. Karlstrom, Y. Asmerom, B. Schmandt, V. Polyak, and S. A. DuFrane (2011), Shrinking of the Colorado Plateau via lithospheric mantle erosion: Evidence from Nd and Sr isotopes and geochronology of Neogene basalts, *Geology*, *39*, 27–30, doi:10.1130/G31611.1.
Currie, C. A., and R. D. Hyndman (2006), The thermal structure of subduction zone back arcs, *J. Geophys. Res.*, *111*, B08404, doi:10.1029/2005JB004024.
Engdahl, E. R., and A. Villasenor (2002), Global seismicity: 1900–1999, in *International Handbook of Earthquake Engineering and Seismology*, vol. 81A, edited by W. H. K. Lee et al., pp. 665–690, Academic, Boston, Mass.
Evans, B., and D. L. Kohlstedt (1995), Rheology of rocks, in *Rock Physics and Phase Relations: A Handbook of Physical Constants*, edited by T. J. Ahrens, pp. 149–165, AGU, Washington, D. C.
Flück, P., R. D., Hyndman, and C. Lowe (2003), Effective elastic thickness *Te* of the lithosphere in western Canada, *J. Geophys. Res.*, *108*(B9), 2430, doi:10.1029/2002JB002201.
François, T., E. B. Burov, B. Meyer, and P. Agard (2013), Surface topography as key constraint on thermo-rheological structure of stable cratons, *Tectonophysics*, *602*, 106–123.
Goetze, C., and B. Evans (1979), Stress and temperature in the bending lithosphere as constrained by experimental rock mechanics, *Geophys. J. R. Astron. Soc.*, *59*, 463–478, doi:10.1111/j.1365-246X.1979.tb02567.x.
Griffin, W. L., S. Y. O'Reilly, N. Abe, S. Aulback, R. M. Davies, N. J. Pearson, B. J. Doyle, and K. Kivi (2003), The origin and evolution of Archean lithospheric mantle, *Precambrian Res.*, *127*, 19–41.
Gueydan F., J. Précigout, and L. Montési (2014), Strain weakening enables continental plate tectonics, *Tectonophysics*, *631*, 189–196.
Handy, M. R., and J.-B. Brun (2004), Seismicity, structure and strength of the continental lithosphere, *Earth Planet. Sci. Lett.*, *223*, 427–441.
Hardebol, N. J., F. Beekman, and S. A. P. L. Cloetingh (2013), Strong lateral strength contrasts in the mantle lithosphere of continents: A case study from the hot SW Canadian Cordillera, *Tectonophysics*, *602*, 87–105.
Hasterok, D., and D. S. Chapman (2011), Heat production and geotherms for the continental lithosphere, *Earth Planet. Sci. Lett.*, *307*, 59–70.
Hyndman, R. D., and C. A. Currie (2011), Why is the North America Cordillera high? Hot backarcs, thermal isostasy, and mountain belts, *Geology*, *39*, 783–786.
Hyndman, R. D., C. A. Currie, and S. Mazzotti (2005), Subduction zone backarcs, mobile belts, and orogenic heat, *GSA Today 15*(2), 4–10, doi:10.1130/1052-5173(2005)015<4:SZBMBA>2.0.CO;2.
Hyndman, R. D., C. A. Currie, S. Mazzotti, and A. Frederiksen (2009), Temperature control of continental lithosphere elastic thickness, *Te vs Vs, Earth Planet. Sci. Lett.*, *277*, 539–548.
Jackson, J. (2002), Strength of the continental lithosphere: Time to abandon the jelly sandwich?, *GSA Today*, *12*(9), 4–10.
Jiménez-Díaz, A., J. Ruiza, M. Pérez-Gussinyé, J. F. Kirby, J. A. Álvarez-Gómez, R. Tejero, and R. Capote (2014), Spatial variations of effective elastic thickness of the lithosphere in Central America and surrounding regions, *Earth Planet. Sci. Lett.*, *391*, 55–66.
Johnston, A. C. (1989), Moment magnitude estimation for stable continental earthquakes, *Seismol. Res. Lett.*, *60*, 1–13.
Johnston, A. C., K. J. Coppersmith, L. R. Kanter, and C. A. Cornell (1994), The earthquakes of stable continental regions, *TR-102261*, Electric Power Res. Inst., Palo Alto, Calif.
Kaban, M. K., M. Tesauro, W. D. Mooney, and S. A. P. L. Cloetingh (2014), Density, temperature and composition of the North American lithosphere: New insights form a joint analysis of seismic, gravity and mineral physics data. Part I: Density structure of the crust and upper mantle, *Geophys. Geochem. Geosyst.*, *15*, 4781–4807, doi:10.1002/2014GC005483.
Kane, M. F., T. G. Hildenbrand, and J. D. Hendricks (1981), A model for the tectonic evolution of the Mississippi Embayment and its contemporary seismicity, *Geology*, *9*, 563–567.
Karato, S.-I., and H. Jung (2003), Effects of pressure on high-temperature dislocation creep in olivine, *Philos. Mag. A*, *83*, 401–414.
Karlstrom, K., and E. Humphreys (1998), Persistent influence of Proterozoic accretionary boundaries in the tectonic evolution of southwestern North America: Interaction of cratonic grain and mantle modification events, *Rocky Mt. Geol.*, *33*(2), 161–179.
Kirby, J. F. (2014), Estimation of the effective elastic thickness of the lithosphere using inverse spectral methods: The state of the art, *Tectonophysics*, *631*, 87–116.
Kirby, J. F., and C. J. Swain (2009), A reassessment of spectral *Te* estimation in continental interiors: The case of North America, *J. Geophys. Res.*, *114*, B08401, doi:10.1029/2009JB006356.

Kirby, J. F., and C. J. Swain (2014), The long-wavelength admittance and effective elastic thickness of the Canadian Shield, *J. Geophys. Res. Solid Earth*, *119*, 5187–5214 doi:10.1002/2013JB010578.
Kreemer, C., G. Blewitt, and E. C. Klein (2014), A geodetic plate motion and global strain rate model, *Geochem. Geophys. Geosyst.*, *15*, 3849–3889, doi:10.1002/2014GC005407.
Lou, X., and S. van der Lee (2014), Observed and predicted North American teleseismic delay times, *Earth Planet. Sci. Lett.*, *402*, 6–15.
Lowry, A. R., and M. Pérez-Gussinyé (2011), The role of crustal quartz in controlling Cordilleran deformation, *Nature*, *471*, 353–357, doi:10.1038/nature09912.
Lowry A. R., and R. B. Smith (1995), Strength and rheology of the western U.S. Cordillera, *J. Geophys. Res.*, *100*, 17,947–17,963.
Lowry A. R., N. M. Ribe, and R. B. Smith (2000), Dynamic elevation of the Cordillera, western United States, *J. Geophys. Res.*, *105*, 23,371–23,390.
Maggi, A., J. A. Jackson, K. Priestley, and C. Backer (2000), A re-assessment of focal depth distribution in southern Iran , the Tien Shan and northern India: Do earthquakes occur in the continental mantle?, *Geophys. J. Int.*, *143*, 629–661.
Mazzotti, S. (2007), Geodynamic models for earthquake studies in intraplate North America, in *Continental Intraplate Earthquakes: Science, Hazard, and Policy Issues, Geol. Soc. Am. Spec. Pap.*, vol. 425, edited by S. Stein and S. Mazzotti, pp. 17–33, doi:10.1130/2007.2425(02).
Mei, S., A. M. Suzuki, D. L. Kohlstedt, N. A. Dixon, and W. B. Durham (2010), Experimental constraints on the strength of the lithospheric mantle, *J. Geophys. Res.*, *115*, B08204, doi:10.1029/2009JB006873.
McKenzie, D. (2003), Estimating Te in the presence of internal loads, *J. Geophys. Res.*, *108*(B9), 2438, doi:10.1029/2002JB001766.
McKenzie, D., and D. Fairhead (1997), Estimates of the effective elastic thickness of the continental lithosphere from Bouguer and free air gravity anomalies, *J. Geophys. Res.*, *102*, 27,523–27,552.
Mooney, W. D. (2015), Global Crustal Structure, in *The Treatise of Geophysics, Crust and Mantle*, 2nd ed., vol. 1, edited by B. Romanowicz and A. Dziewonski, pp. 361–417, Elsevier, Amsterdam.
Mooney, W. D., and M. K. Kaban (2010), The North American upper mantle: Density, composition, and evolution, *J. Geophys. Res.*, *115*, B12424, doi:10.1029/2010JB000866.
Mooney, W. D., J. Ritsema, and Y. Keun Hwang (2012), Crustal seismicity and the earthquake catalog maximum moment magnitude (Mcmax) instable continental regions (SCRs): Correlation with the seismic velocity of the lithosphere, *Earth Planet. Sci. Lett.*, *357–358*, 78–83.
Mouthereau, F., A. Watts, and E. Burov (2013), Structure of orogenic belts controlled by lithosphere age, *Nat. Geosci.*, *6*, 785–789, doi:10.1038/ngeo1902.
Nolet, G. (1990), Partitioned waveform inversion and two-dimensional structure under the network of autonomously recording seismographs, *J. Geophys. Res.*, *95*, 8499–8512.
Parsons, T., G. A. Thompson, and N. H. Sleep (1994), Mantle plume influence on the Neo gene uplift and extension of the U.S. western Cordillera, *Geology*, *22*, 83–86.
Pilkington, M. (1991), Mapping elastic lithospheric thickness variations in Canada, *Tectonophysics*, *190*, 283–297.
Pollack, H. N., and D. S. Chapman (1977), On the regional variation of heat flow, geotherms and lithospheric thickness, *Tectonophysics*, *38*, 279–296.
Poudjom Djomani, Y. H., W. L. Griffin, S. Y. O'Reilly, and B. J. Doyle (2005), Lithospheric domains and controls on kimberlite emplacement, Slave province, Canada: Evidence from elastic thickness and upper mantle composition, *Geochem. Geophys. Geosyst.*, *6*, Q10006, doi:10.1029/2005GC000978.
Ranalli, G. (1994), Nonlinear flexure and equivalent mechanical thickness of the lithosphere, *Tectonophysics*, *240*(1), 107–114.
Rippe, D., M. J. Unsworth, and C. A. Currie (2013), Magnetotelluric constraints on the fluid content in the upper mantle beneath the southern Canadian Cordillera: Implications for rheology, *J. Geophys. Res. Solid Earth*, *118*, 5601–5624, doi:10.1002/jgrb.50255.
Roy, M., T. H. Jordan, and J. Pederson (2009), Colorado Plateau magmatism and uplift by warming of heterogeneous lithosphere, *Nature*, *459*, 978–982, doi:10.1038/nature08052.
Schaeffer, A. J., and S. Lebedev (2013), Global shear-speed structure of the upper mantle and transition zone, *Geophys. J. Int.*, *194*(1), 417–449.
Schmandt, B., and E. Humphreys (2010), Complex subduction and small-scale convection revealed by body wave tomography of the western United States, *Earth Planet. Sci. Lett.*, *297*, 435–445, doi:10.1016/j.epsl.2010.06.047.
Schulte, S., and W. D. Mooney (2005), An updated global earthquake catalogue for stable continental regions: Reassessing the correlation with ancient rifts, *Geophys. J. Int.*, *161*, 707–721.
Sloan, R. A., J. A. Jackson, D. McKenzie, and K. Priestley (2011), Earthquake depth distributions in central Asia, and their relations with lithosphere thickness, shortening and extension, *Geophys. J. Int.*, *185*, 1–29.
Stixrude, L., and C. Lithgow-Bertelloni (2005), Thermodynamics of mantle minerals—I: Physical properties, *Geophys. J. Int.*, *162*, 610–632.
Tesauro, M., M. K. Kaban, and S. A. P. L. Cloetingh (2009a), A new thermal and rheological model of the European lithosphere, *Tectonophysics*, *476*, 478–495.
Tesauro, M., M. K. Kaban, and S. A. P. L. Cloetingh (2009b), How rigid is Europe's lithosphere?, *Geophys. Res. Lett.*, *36*, L16303, doi:10.1029/2009GL039229.
Tesauro, M., M. K. Kaban, and S. A. P. L. Cloetingh (2010), Thermal and rheological model of the European lithosphere, in *New Frontiers in Integrated Solid Earth Sciences New Frontiers in Integrated Solid Earth Sciences*, edited by S. A. P. L. Cloetingh and J. F. W. Negendank, pp. 71–101, Springer, Berlin.
Tesauro, M., M. K. Kaban, and S. A. P. L. Cloetingh (2012a), Global strength and elastic thickness of the lithosphere, *Global Planet. Change*, *90–91*, 51–57.
Tesauro, M., P. Audet, M. K. Kaban, R. Bürgmann, and S. A. P. L. Cloetingh (2012b), The effective elastic thickness of the continental lithosphere: Comparison between rheological and inverse approaches, *Geochem. Geophys. Geosyst.*, *13*, Q09001, doi:10.1029/2012GC004162.
Tesauro, M., M. K. Kaban, and S. A. P. L. Cloetingh (2013), Global model for the lithospheric strength and effective elastic thickness, *Tectonophysics*, *602*, 78–86.
Tesauro, M., M. K. Kaban, W. D. Mooney, and S. A. P. L. Cloetingh (2014a), Density, temperature and composition of the North American lithosphere: New insights form a joint analysis of seismic, gravity and mineral physics data. Part II: Thermal and compositional model of the upper mantle, *Geophys. Geochem. Geosyst.*, *15*, 4808–4830, doi:10.1002/2014GC005484.
Tesauro, M., M. K. Kaban, W. D. Mooney, and S. A. P. L. Cloetingh (2014b), A 3D model for the crustal structure of the North American Continent, *Tectonophysics*, *631*, 65–86.
Triep, E. G., and L. R. Sykes (1996), Catalog of shallow intracontinental earthquakes. [Available at http://www.ldeo.columbia.edu/seismology/triep/intra.expl.htmlS.]

Turcotte, D. L., and G. Schubert (2014), Geodynamics, Cambridge University, 636 pp.
van der Lee, S., K. Regenauer-Lieb, and D. A. Yuen (2008), The role of water in connecting past and future episodes of subduction, *Earth Planet. Sci. Lett.*, *273*, 15–27.
Wang Y., and J. C. Mareschal (1999), Elastic thickness of the lithosphere in the central Canadian Shield, *Geophys. Res. Lett.*, *26*, 3033–3036.
Watts, A. B., and E. V. Burov (2003), Lithospheric strength and its relationship to the elastic and seismogenic layer thickness, *Earth Planet. Sci. Lett.*, *213*, 113–131.
Watts A. B., and S. Zhong (2000), Observations of flexure and the rheology of oceanic lithosphere, *Geophys. J. Int.*, *142*, 855–875.
Wiens, D. A., and S. Stein (1983), Age dependence of oceanic intraplate seismicity and implications for lithospheric evolution, *J. Geophys. Res.*, *88*, 6455–6468.
Wilks, K. R., and N. L. Carter (1990), Rheology of some continental lower crustal rocks, *Tectonophysics*, *182*, 57–77.
Yaolin, S., and C. Jianling (2008), Lithosphere effective viscosity of continental China, *Earth Sci. Front.*, *15*(3), 82–95.